

CD95L mRNA and CD95L derived si- and shRNAs kill cancer cells through an RNAi mechanism by targeting survival genes

William Putzbach^{1,6}, Quan Q. Gao^{1,6}, Monal Patel^{1,6}, Abbas Hadji^{1,7}, Stijn van Dongen⁴, Ashley Haluck-Kangas¹, Elizabeth Bartom², Austin Stults¹, Abdul S. Qadir¹, Kwang-Youn A. Kim³, Markus Hafner⁵, Jonathan C. Zhao¹, Andrea E. Murmann¹ and Marcus E. Peter^{1,2,*}

¹Division Hematology/Oncology and ²Department of Biochemistry and Molecular Genetics, ³Department of Preventive Medicine, Feinberg School of Medicine, Northwestern University, Chicago, IL 60611, USA; ⁴European Bioinformatics Institute (EMBL-EBI), Hinxton, Cambridge CB10 1SD, UK; ⁵NIAMS/NIH, Bethesda, MD 20892

Corresponding author: Marcus Peter, E-mail: m-peter@northwestern.edu, phone: 312-503-1291; FAX: 312-503-0189.

⁶ Shared first authorship

⁷ Current address: Department of Pediatrics, Section of Hematology/Oncology/Stem Cell Transplantation, University of Chicago, Chicago, IL 60637

Keywords:

RNAi, Fas, cancer, CRISPR, cell death, DISE

Abstract

Immune cells kill tumour cells by activating the CD95/Fas death receptor triggering apoptosis. Unexpectedly however, >80% of a large number of siRNAs and shRNAs tested targeting CD95 or CD95 ligand (CD95L) induce a robust form of cell death that is characterized by the simultaneous activation of multiple death pathways and preferentially affects transformed and cancer stem cells. We now show that si/shRNAs derived from CD95 or CD95L are toxic to cancer cells through canonical RNAi by targeting the 3'UTR of critical survival genes in a unique form of off-target effect. By testing 4666 shRNAs derived from the CD95 and CD95L mRNAs and an unrelated control gene, Venus, we have located the most toxic sequences in the open reading frame of CD95L. Consistently, CD95L mRNA is highly toxic to cancer cells after complete deletion of CD95. Our data provide the first evidence for mRNAs to affect cell fate through RNAi in mammalian cells. In addition, they suggest that cancer cells can be targeted with specific toxic RNAi active sequences present in the genome.

CD95 (Fas/APO-1) is a death receptor that when bound by its ligand, CD95L, mediates induction of apoptosis, most prominently in the context of the immune system¹. However, in recent years it has become apparent that the CD95/CD95L system has multiple tumour-promoting activities². CD95 signalling promotes cell growth³, increases motility and invasiveness of cancer cells^{4,5}, and promotes cancer stemness⁶⁻⁸. In fact, we reported that tumours after deleting the CD95 gene barely grew in vivo^{3,9}. Therefore, it appeared consistent when we discovered that multiple shRNAs and siRNAs targeting either CD95 or CD95L slowed down cancer cell growth³ and engaged a form of cell death that was found to be a combination of multiple cell death pathways⁹; it could not be inhibited by conventional cell death or signalling pathway inhibitors or by knockdown of any single gene in the human genome⁹; it preferentially affected transformed cells⁹ and among them cancer stem cells⁶.

One of the most widely used methods to reduce expression of genes in cells is RNA interference (RNAi) which has been used to identify genes that are critical for the survival of human cancer cell lines⁹⁻¹². During RNAi, small interfering (si)RNAs, small hairpin (sh)RNAs or micro (mi)RNAs inhibit gene expression. miRNAs are generated as primary transcripts in the nucleus, undergo processing to pre-miRNAs by the Drosha-DGCR8 complex before being exported to the cytosol by exportin 5^{13,14}. siRNAs are produced from both shRNAs and miRNAs when the RNase III, Dicer in complex with TRBP, cleaves double-stranded (ds)RNA into 21-23 nucleotide long fragments that have a two nucleotide 3' overhang¹⁵. DsRNA fragments or chemically synthesized siRNAs are loaded into the RNA-induced silencing complex (RISC)¹⁶. A near-perfect complementary between the guide strand of the si/miRNA and the target mRNA sequence results in cleavage of the mRNA¹⁷. Incomplete complementarity results in inhibition of protein translation, and contributes to mRNA degradation¹⁸. mRNA targeting is mostly determined by the seed sequence, positions 2-7/8 of the guide strand, which is fully complementary to the seed match in the 3'UTR of targeted mRNAs. Similar to miRNAs, although not fully explored, siRNAs and shRNAs also target multiple other mRNAs besides the mRNAs they were designed to silence, a phenomenon commonly referred to as off-target effect (OTE) that is generally sought to be avoided¹⁹⁻²¹.

si/shRNAs kill cells in the absence of the targeted site.

We previously demonstrated more than 80% of a large number of tested shRNAs or siRNAs designed to target either CD95 or CD95L were toxic to multiple cancer cells⁹ (**Fig. S1a**). We have now extended this analysis to DICER substrate 27mer DsiRNAs²². All DsiRNAs designed to target CD95L displayed toxicity when introduced into HeyA8 cells at 5 nM (**Fig. S1b**) reinforcing our previous observation that the majority of CD95 and CD95L targeting sh- and siRNAs are toxic to cancer cells. From our own experience and from multiple published genome-wide RNAi screens⁹⁻¹² it appears that only a small fraction (between 2% and 5%) of si/shRNAs are usually toxic. This toxicity could in part be due to an OTE. However, the high percentage of toxic si/shRNAs derived from CD95 and CD95L seemed to exclude an OTE and pointed at a survival activity of CD95 and CD95L. This interpretation at least for the CD95 was supported by our data on tissue-specific deletion of CD95 to attenuate or prevent tumour formation in mouse tumour models^{3,9}.

However, the toxic activity of the CD95L targeting si/shRNAs was puzzling considering that in most cancer cells tested CD95L was not expressed⁹. Consistent with this observation we could not rescue cells from cell death by treating them with recombinant CD95L after introduction of CD95L targeting shRNAs (**supplementary results and Fig. S2a**). Most

strikingly introducing siRNA resistant versions of CD95L or CD95 did also failed to protect cells from the toxic effects of CD95L and CD95 targeting shRNAs, respectively (**supplementary results** and **Fig. S2b-2g**).

To determine whether the targeted sites in CD95 and CD95L were actually required for the shRNAs to kill we used CRISPR/Cas9 gene editing to excise sites targeted by different shRNAs and siRNAs in both alleles of the CD95 and CD95L genes. We first deleted a 41 nt piece of the CD95L gene in 293T cells, that contained the target site for shL3 (**Fig. 1a, 1c**). While internal primers could not detect CD95L mRNA in three tested clones, primers outside of the deleted area did detect CD95L mRNA (**Fig. 1d**, and data not shown). Three clones with this shL3 Δ 41 deletion were pooled and tested for toxicity by shL3 expressed from a Tet-inducible plasmid (pTIP-shL3). Compared to a pool of control cells transfected only with the Cas9 plasmid, the 293T shL3 Δ 41 cells were equally sensitive to the toxic shRNA (**Fig. 1g**). This was also observed when the clones were tested individually (data not shown).

To exclude the possibility that shL3 was inducing cell death due to an activity unique to shL3 and/or 293T cells, we deleted the same 41 nt in CD95L in the ovarian cancer cell line HeyA8; We also removed 64 nt containing the target site for the siRNA siL3 in the CD95L coding sequence, and a 227 nt region containing the target site for shR6 in CD95 in HeyA8 cells (**Fig. 1a, 1b** and **Fig. S3**). In all cases homozygous deletions were generated (**Fig. 1e**). To confirm the deletion of the shR6 target site, we infected HeyA8 cells treated with the Cas9 plasmid only and HeyA8 with the deleted shR6 site with shR6, shR2 (both targeting the CD95 ORF) and shR6' (targeting the CD95 3'UTR). Five days after infection, CD95 mRNA was quantified by real time PCR (**Fig. 1f**). Using a primer located outside the 227bp deletion, the mutated CD95 mRNA was still detectable in the cells. While shR2 and shR6' caused knockdown of CD95 mRNA in both the Cas9 expressing control and the R6 Δ 227 k.o. cells, shR6 could only reduce mRNA expression in the parental cells. These data document that HeyA8 CD95 shR6 Δ 227 cells no longer harbour the sequence targeted by shR6.

Now having HeyA8 cells lacking one of three RNAi targeted sites in either CD95 or CD95L, we could test the role of the CD95 and CD95L genes in protecting HeyA8 cells from the death induced by either shRNAs (shL3 and shR6, two different vectors: pLKO or the Tet inducible pTIP) or the siRNA siL3. In all cases, the shRNA or siRNA that targeted the deleted region was still fully toxic to the target-site deleted cells (**Fig. 1h** and **1i**). In the siL3 target site deleted cells, we could titre the amount of siL3 needed to kill the cells. We saw efficient growth reduction and cell death in cells transfected with as little as 1 nM, well below the commonly used and recommended concentration of siRNAs (5-50 nM) (**Fig. 1i**, and data not shown). These data firmly establish that cells were not dying due to targeting either CD95 or CD95L.

Involvement of canonical RNAi.

shRNAs and early generation naked siRNAs showed general toxicity when introduced in large amounts, presumably by eliciting an interferon (IFN) response²³ or by saturating the RISC²⁴. However, both chemically modified siRNAs at very low concentrations and lentiviral shRNAs at an MOI<1 cells were still toxic (data not shown). We therefore decided to test whether the observed toxicity involved canonical RNAi and activity of the RISC. To be able to test all possible shRNAs or siRNAs targeting CD95L, we generated a sensor plasmid, comprised of Venus followed by the ORF of CD95L (inset in **Fig. 2a**). To minimize production of functional CD95L protein we deleted the first A in the ATG start codon of the CD95L cDNA in the sensor. Likely due to a small amount of CD95L still produced from the CD95L sensor, HeyA8 cells infected with this sensor virus slowed down in growth and some cells died by apoptosis (data not shown). We therefore used the CD95 protein k.o. cells we had generated in the process of

deleting the shR6 site (**Fig. S3**, clone # 2 was used for the following studies, see figure legend for strategy and characterization of the clones). While ds-siL3 effectively silenced Venus expression and induced toxicity, neither the sense nor the antisense single stranded (ss)RNAs significantly affected Venus expression or toxicity (**Fig. 2a**). In addition, no activity was found when ds-siL3 was transfected into the cells synthesized as deoxyribo-oligonucleotides (**Fig. 2b**). Using this type of analysis, we tested a number of modified siRNAs. For siRNAs to be fully active they require 3' overhangs in both strands. Converting siL3 to a blunt-end duplex resulted in a substantial loss of RNAi activity and toxicity (**Fig. 2c**). Due to the topology of the RISC siRNA activity is decreased by modification of the 5' end of the antisense/guide strand. To test whether cell death induced by siL3 was affected by a bulky modification, we placed a Cy5 moiety at either of the four possible ends of the siL3 duplex. Only when the siL3 duplex carried a 5' modification in the guide strand did it prevent RNAi activity and toxicity, modifications in the three other positions had no effect (**Fig. 2c**). This was confirmed for another siRNA, siL2. To test whether the toxicity of siL3 required association with the macromolecular complex consistent with RISC involvement, we performed a competition experiment. HeyA8 cells were transfected with 10 nM of siL3, and a mutated nontoxic oligonucleotide, siL3MUT, was titrated in (**Fig. 2d**). siL3MUT reduced the growth inhibitory activity of siL3 in a dose-dependent fashion suggesting that both siL3 and siL3MUT compete for the same binding site in the cells, pointing at involvement of the RISC.

To determine the involvement of components of the RNAi pathway in the toxicity of shRNAs we tested HCT116 cells deficient for either Drosha or Dicer²⁵. Growth of parental HCT116 cells was impaired after infection with shL3 or shR6 viruses (**Fig. 2e**, left panel). Consistent with the requirement of Dicer to process shRNAs Dicer k.o. cells were completely resistant to the toxic shRNAs (**Fig. 2e**, centre panel). This was also supported by the inability of shR6 to silence CD95 protein expression (**Fig. 2f**). Dicer^{-/-} cells were not resistant to toxic siRNAs as these cells died when transfected with siL3, which does not depend on Dicer for processing (**Fig. 2g**). Interestingly, Drosha^{-/-} cells were hypersensitive to the two toxic shRNAs (**Fig. 2e**, right panel) and shR6 efficiently knocked down CD95 expression in Drosha^{-/-} cells (**Fig. 2f**). Both Drosha^{-/-} and Dicer^{-/-} cells were more susceptible to the toxicity induced by siL3 than parental cells (**Fig. 2g**). The hypersensitivity of the Drosha^{-/-} cells to toxic si/shRNAs and of Dicer^{-/-} cells to toxic siRNAs is consistent with a model in which toxic shRNAs require RISC to kill cells and Drosha^{-/-} and Dicer^{-/-} cells which are almost completely devoid of miRNAs²⁵ allow much more efficient uptake of the toxic si/shRNAs into the RISC.

To test what the contribution of the seed sequence in the siRNAs are to their toxicity we generated a set of chimeric siRNAs in which we replaced nucleotides of the toxic siL3 siRNA with nucleotides of a nontoxic scrambled RNA. We did this starting either from the seed end or from the opposite end (**Fig. 2i**). HeyA8 cells expressing both the Venus-CD95L sensor (to monitor level of knockdown) and a Nuc-Red plasmid to fluorescently label nuclei (to monitor the effects on cell growth) were transfected with 5 nM of the chimeric siRNAs; total green fluorescence and the number red fluorescent nuclei were quantified over time. The siL3 control transfected cells showed an almost complete suppression of the green fluorescence and high toxicity. In the top panel of **Fig. 2i** the data are summarized in which siL3 nucleotides were stepwise replaced with siScr nucleotides from the seed match end. Both RNAi and toxicity were profoundly reduced when three of the terminal siL3 nucleotides were replaced with the siScr nucleotides in those positions suggesting that the seed region (6mer shown in blue) is critical for both activities (top panel in **Fig. 2i**). Consistently, when siL3 nucleotides were replaced with siScr nucleotides from the non-seed end, neither RNAi nor the toxicity was diminished until replacements affected residues in the seed region (bottom panel in **Fig. 2i**). These data suggest

that a 6mer seed sequence of siL3 is critical for its CD95L specific RNAi activity and also its toxicity. These data provide strong evidence that the toxicity observed is a sequence specific event, and not the result of general toxicity resulting from a toxic sequence motif in the siRNA, or from poisoning the RISC. Rather, this toxicity follows the rules of canonical RNAi.

Importance of seed sequences in the guide RNA.

A general OTE by RNAi has been reported¹⁹⁻²¹. However, this has not been found to cause toxicity in most cases and the targeted mRNAs were difficult to predict²⁰. The fact that 22 of the tested CD95 and CD95L targeting sh- and si/DsiRNAs were toxic to many cancer cells and that in affected cells and evoked similar morphological and biological responses in cells⁹ generated a conundrum: Could an OTE trigger a specific biology? In order to test this we expressed two shRNAs - one targeting CD95L (shL3) and one targeting CD95 (shR6) - in cells lacking their respective target sequences and subjected the RNA isolated from these cells to an RNA-Seq analysis. In order to detect effects that were independent of cell type, delivery of the shRNA, or targeted gene, we expressed shL3 in 293T (Δ shL3) cells using the Tet inducible vector pTIP and shR6 in HeyA8 (Δ shR6) cells using the pLKO vector. In each case, changes in RNA abundance were compared to cells in which we expressed a non-targeting shRNA in matching vectors. Total RNA was harvested in all cases at either the 50 hour time point (before the onset of cell death) or at the 100 hour time point (during cell death) (**Fig. 3a**). In order to achieve high stringency, the data were then analysed in two ways: first, using a conventional alignment-based analysis to identify genes for which the mRNA changed more than 1.5 fold (and an adjusted p-value of less than 0.05) and second, by a read-based method, in which we first identified all reads that changed >1.5 fold and then subjected each read to a BLAST search to identify the gene it was derived from. Only RNAs that were detected by both methods were considered (**Table S1**). The combination of the analyses resulted in one RNA that was upregulated and 11 mRNAs that were downregulated (**Fig. 3b**). Using an arrayed qPCR approach, most of these detected mRNA changes were validated for both cell lines (**Fig. S4a**). Interestingly, for nine of the eleven genes, published data suggested that they are either highly upregulated in cancer and/or critical for the survival of cancer cells as their inhibition or knockdown resulted in either growth reduction or induction of various forms of cell death (**supplementary results**). Significantly, six of these eleven downregulated genes were recently identified in two genome-wide RNAi independent lethality screens to be critical for the survival of cancer cell lines^{10,26} (**Fig. 3b** and **Fig. S4b**) (**Table S2**). Considering that these two screens only identified 6.6% of human genes to be critical for cell survival, we found a significant enrichment (54.5%, $p < 0.0001$) of these survival genes among the genes downregulated during the cell death induced by either shL3 or shR6. All six survival genes are either highly amplified or mutated in human cancers (**Fig. S5a**). In addition to these six genes, GNB1 and HIST1H1C were reported to be required fitness genes in recent high-resolution CRISPR-based screen²⁷. A kinetic analysis showed that most of the deregulated mRNAs were downregulated early with a strong effect at around 26 hours, two days before the onset of cell death (**Fig. S4c**). This suggested that the cells were dying because of the silencing of multiple critical survival genes providing an explanation for why multiple cell death pathways were activated. We are therefore calling this type of cell death DISE (for death induced by survival gene elimination).

To confirm that some of the downregulated genes were survival genes for HeyA8 cells, we transfected the cells with siRNA SmartPools targeting each of the eleven genes. Individual knockdown of seven of the targeted genes resulted in reduced cell growth when compared to cells transfected with a pool of scrambled siRNAs (**Fig. 3c**). To mimic the effect of the CD95 and CD95L-derived shRNAs, we treated HeyA8 cells with a combination of siRNA pools

targeting these seven genes. Remarkably, 1 nM of this siRNA mixture (35.7 pM of each individual siRNA) was sufficient to effectively reduce cell growth in these cells (**Fig. S5b**) and to cause substantial cell death (**Fig. S5c**), suggesting it is possible to kill cancer cells with very small amounts of siRNAs targeting a network of these survival genes.

To test whether the introduced CD95 and CD95L-derived shRNAs directly targeted genes through canonical RNAi, we subjected two gene lists obtained from the RNA-Seq analysis (both cell lines at the 50 hour time point) to a Sylamer analysis²⁸ designed to find an enrichment of miRNA/shRNA targeted sites in the 3'UTR of a ranked list of genes (**Fig. 3d**). This analysis identified a strong enrichment of the cognate seed match for shL3 and shR6 in cells treated with one of these two shRNAs. The analyses with cells treated with shRNAs for 100 hours looked similar but less significant, suggesting early targeting by the shRNAs followed by secondary events (data not shown). Enrichment in 6mers and 8mers were both detected (only 8mers shown) in the 3'UTRs but not the ORF of the ranked genes (data not shown). Interestingly, the detected seed matches were shifted by one nucleotide from the expected seed match based on the 21mer coded by the lentivirus. RNA-Seq analysis performed for the small RNA fraction confirmed that in all cases (shScr and shL3 in pTIP, and shScr and shR6 in the pLKO vector) the shRNAs in the cells were being cleaved in a way that resulted in the predominant formation of an siRNA that was shifted one nucleotide away from the shRNA loop region (black arrow heads in **Fig. S6a**). This allowed us to design toxic siRNAs based on the sequences of shL3 and shL6. These shRNA-to siRNA converts were toxic to HeyA8 cells (**Fig. S6b**) confirming that the observed toxicity was not limited to the TRC shRNA platform but based on a sequence specific activity of the sh/siRNAs.

It has been reported that in siRNA overexpression experiments, changes in mRNA expression can be caused by blocked access of endogenous miRNAs to the RISC, such as the highly expressed miRNA family, let-7²⁹. However, we can exclude such an effect in our analysis, as there was no significant enrichment (or depletion) of the let-7 seed match motif (or that of any other miRNA) in our analyses (black lines in **Fig. 3d**). It is more likely that the two shRNAs, shL3 and shR6, targeted a network of genes enriched in critical survival genes, and indeed, in 10 of the 11 targeted genes, 6mer seed matches for either shL3 or shR6 (as determined by the Sylamer and RNA Seq analyses) could be found (labelled in **Fig. 3b**). To test the generality of this phenomenon we inducibly expressed another CD95L derived shRNA, shL1 in 293T cells using the pTIP vector, transfected HeyA8 cells with 25 nM siL3 and subjected the cells to RNA-Seq analysis 100 hours and 48 hours after addition of Dox or after transfection, respectively. In both cases when the ranked RNA Seq data were subjected to a Sylamer analysis the seed matches of the sh/siRNA introduced was significantly enriched in the 3'UTR of downregulated RNAs (**Fig. S6c**). In none of the Sylamer analyses of the four data sets did we see enrichment of seed matched in the 3'UTR of downregulated RNAs that matched the passenger strand. In all cases the only significantly enriched sequences matched the seed sequences in the guide RNA of the sh- and siRNAs. This suggests that the observed toxicity was not the result of passenger strand loading, one of the mechanisms that has been implicated in OTE of RNAi³⁰.

Downregulation of survival genes.

In order to determine whether survival genes were downregulated in all four cases of sh/siRNAs induced cell death, we used a list of 1883 survival genes and 423 genes not required for survival (nonsurvival genes) recently identified in a CRISPR lethality screen (**Table S2**). We subjected the four ranked RNA Seq data sets to a gene set enrichment analysis using the two gene sets (**Fig. 3e**). In all four cases survival genes were significantly enriched towards the top of the ranked lists. In contrast, nonsurvival genes were not enriched. One interesting feature of DISE

that emerged was the substantial loss of histones. Of the 16 genes that were significantly downregulated in cells treated with four sh/siRNAs, 12 were histones (**Fig. 3f**). Only four of these histones have a 3'UTR (underlined in **Fig. 3f**) suggesting that most histones are not directly targeted by the sh/siRNAs.

To determine whether the survival genes could be downregulated due to a direct targeting by each sh/siRNAs we determined for each treatment whether there was a connection between the presence or absence of a predicted seed match of the sh/siRNA introduced and the significance of downregulation (>1.5 fold downregulated, $p < 0.05$) among survival genes using the Fisher's Exact test (**Fig. 3g**). In almost all cases this analysis revealed that survival genes containing a predicted seed match in their 3'UTR were statistically more likely to be selectively downregulated than survival genes without such a motif. The analysis with shL1 treated cells did not reach statistical significance, likely due to the fact that this shRNA was found to be very toxic and the 100 hour time point may have been too late to observe evidence of significant targeting. This interpretation is supported by the observation that the significance for both shL3 and shR6 to target survival genes was higher at 50 hours when compared to the 100 hour time points (**Fig. 3g**) and that the Sylamer analysis of the shL1 treated cells was less significant after 100 hours of treatment than any of the other Sylamer analyses (**Fig. S6C**). We noticed that the survival genes were more highly expressed than the nonsurvival genes (data not shown). To compensate for this difference, we chose for each of the 1210 survival genes identified in the two studies^{10,26} and expressed in HeyA8 and 293T cells an expression-matched gene that is not critical for survival (data not shown). We then identified all genes in each group that had read numbers of at least 100 in any of the 16 control treated cells in our RNA seq analyses. Finally, we ranked all significantly expressed genes (average read numbers of at least 1000) according to the length of its 3'UTR and highlighted the location of each survival gene (SG) and expression-matched nonsurvival gene (nonSG). Interestingly, the SGs trended to have shorter 3'UTRs than the expression-matched nonSGs. This may suggest an evolutionary selection pressure on SGs to have shorter 3'UTRs consistent with a regulation through their 3'UTRs. Overall analyses suggested that cells die by DISE due to an early silencing of survival genes through targeting seed matches in their 3'UTR followed by the downregulation of histones.

Identification of toxic shRNAs in the CD95L and CD95 mRNAs.

The majority of commercially available si-, Dsi-, and shRNAs derived from either CD95 or CD95L were highly toxic to cancer cells. We therefore asked whether these two genes contained other sequences with a similar activity. In order to test all shRNAs derived from either CD95L or CD95, we synthesized all possible shRNAs, 21 nucleotides long, present in the ORF or the 3'UTR of either CD95L or CD95 starting with the first 21 nucleotides after the start codon, and then shifting the sequence by one nucleotide along the entire ORF and 3'UTR (**Fig. 4a**). We also included shRNAs from a gene not expressed in mammalian cells and not expected to contain toxic sequences, Venus. All 4666 oligonucleotides (700 Venus, 825 CD95L ORF, 837 CD95L 3'UTR, 987 CD95 ORF, and 1317 CD95 3'UTR shRNAs) were cloned into the Tet inducible pTIP vector (**Fig. 4b**) as five individual pools. We first tested the activity of each pool to be toxic and to target the Venus sensor protein (fused to either the ORF of CD95 or CD95L). NB7 neuroblastoma cells were chosen for these experiments because they lack expression of caspase-8³¹ and hence are completely resistant to the apoptosis inducing effects of CD95L. NB7-Venus-CD95L cells infected with the Venus-targeting shRNA pool showed some reduction in fluorescence when Dox was added, however, the shRNA pool derived from the CD95L ORF was much more active in knocking down Venus (**Fig. S7a**). No significant green fluorescence reduction was detected in cells after infection with the shRNA pool derived from the CD95L

3'UTR since the targeted sequences were not part of the sensor. Similar results were obtained when NB7-Venus-CD95 cells were infected with the Venus, CD95 ORF, and CD95 3'UTR targeting shRNA pools. To determine the ability to reduce cell growth (as a surrogate marker for toxicity), we infected NB7 parental cells with each of the five pools (parental cells were used to avoid a possible sponge effect by expressing either CD95L or CD95 sequences that were part of the Venus sensors). Interestingly, the pool of 700 shRNAs derived from Venus did not cause any toxicity (**Fig. S7b**). In contrast, the pool of the shRNAs derived from CD95L significantly slowed down growth, while no toxicity was observed when cells were infected with the pool of shRNAs derived from the CD95L 3'UTR. In the case of CD95, both the shRNAs derived from the ORF and the 3'UTR showed some toxicity. However, the shRNAs derived from the 3'UTR caused greater toxicity compared to those derived from the ORF. The data suggests that overall the shRNAs derived from the CD95L ORF and the CD95 3'UTR contain the most toxic shRNAs.

To determine the toxicity of each of the shRNAs in the pools, NB7 cells were infected with each library of shRNA viruses (MOI<1), and after puromycin selection cells were pooled 1:1:1 (Venus ORF/CD95L ORF/CD95L 3'UTR pools or Venus ORF/CD95 ORF/CD95 3'UTR pools) to allow for competition between shRNAs when Dox was added (**Fig. 4b**). Cells were cultured for 9 days with and without Dox to allow for cell death to occur. Next generation sequencing was performed on a PCR fragment containing the shRNA barcode (isolated from genomic DNA) to determine the relative abundance of each shRNA in three pools: 1) the cloned plasmid libraries, 2) cells after infection and culture for 9 days without Dox, and 3) cells infected and cultured with Dox for 9 days. A total of 71,168,032 reads were detected that contained a complete sequence of one of the cloned shRNAs. Almost all shRNAs were represented in the cloned plasmids (**Table S3**). The shRNAs in the CD95L pool (comprised of the Venus, CD95L ORF, and CD95L 3'UTR subpools) and the CD95 pool (comprised of the Venus, CD95 ORF, and CD95 3'UTR subpools) were ranked from highest (most toxic) to lowest underrepresentation. During this and subsequent analyses we noticed that in many cases Dox addition did cause a reduction of shRNAs, indicating an increase in toxicity; However, in other cases infection alone without the addition of Dox was toxic. This effect was likely due to the well-described leakiness of the Tet-on system³² which we confirmed for the shR6 shRNA (**Fig. S8a**). To capture all toxic shRNAs, we therefore decided to split the analyses into two halves: 1) the changes in abundance after infection (infection -Dox) and 2) the changes in abundance after Dox addition (infection +Dox). The results for all shRNAs are shown in **Fig S8b**. Grey dots represent all shRNAs and red dots represent only the ones that were significantly underrepresented at least 5 fold. Interestingly, the highest abundance of downregulated shRNAs was found in the CD95L ORF and the CD95 3'UTR pools of shRNAs, which is consistent with the increased toxicity that was observed when NB7 cells were infected with either of these two pools (see **Fig. S7b**). The shRNAs of these two toxic pools were highly enriched in the underrepresented shRNAs in the two pooled experiments (CD95L and CD95). Their toxicity was also evident when all shRNAs in each pool (2362 shRNAs in the CD95L and 3004 shRNAs in the CD95 pool) were ranked according to the highest fold downregulation (**Fig. 4c**). The three subpools in each experiment are shown separately; Again this analysis identified the subpools with the highest enrichment of underrepresented shRNAs as the ORF of CD95L and the 3'UTR of CD95 (**Fig. 4c**). In both analyses, the one with shRNAs underrepresented after infection due to vector leakiness is boxed in blue and the ones after Dox addition is boxed in orange.

This analysis allowed us to describe the toxicity landscape of CD95L and CD95 ORFs and their 3'UTRs (**Fig. 4d**). All shRNAs that were significantly underrepresented at least five fold (red dots in **Fig. S8b**) are shown along the CD95L pool (**Fig. 4d, left**) and the CD95 pool (**Fig. 4d, right**) sequences. Blue marks show underrepresented shRNAs after infection, and orange

marks show underrepresented shRNAs after 9 days culture with Dox. For both CD95L and CD95, toxic shRNAs were located in distinct clusters.

Our data suggest that toxic shRNAs derived from either CD95L or CD95 kill cancer cells by targeting a network of genes critical for survival through canonical RNAi. Therefore, we wondered how many 8mer seed sequences derived from these toxic shRNAs would have corresponding seed matches in the 3'UTR of critical survival genes in the human genome. shRNAs containing these sequences could potentially be toxic to cells. To calculate such a hypothetical toxicity index, we used the ranked CRISPR data set¹⁰ with 1883 SGs and 423 nonSGs. Based on our RNA Seq analyses, we hypothesized that the survival genes contained more putative seed matches of the shRNA in their 3'UTRs than the nonsurvival genes. We found 3'UTR information of 1846 of the survival genes and 416 of the nonsurvival genes.

In order to establish a Toxicity Index (TI) for each shRNA, we first generated a list containing a normalized ratio of occurrences of any possible 8mer seed match in the 3'UTRs of the survival and non-survival gene groups. This resulted in a ratio for each of the 65,536 possible 8mer combinations (**Table S4**), the TI. We then assigned to each of the 4666 shRNAs in our screen its TI and ranked each pool within the two experiments of our screen according to the highest TI and again separated the two groups of shRNAs, that were toxic just after infection and after addition of Dox (**Fig. 4e**) (**Table S5**). In each ranked list, we could now assess whether the experimentally determined toxicity of shRNAs correlated with the *in silico* predicted TI. Remarkably, the highest enrichment of toxic shRNAs was found amongst those with higher TI for the subpool of shRNAs targeting the CD95L ORF followed by shRNAs in the subpool targeting the CD95 3'UTR. To confirm the significance of this finding, we repeated the analysis 10,000 times by randomly assigning 8mers and their associated TIs to the two shRNA pools and again sorted the data from highest to lowest TI. The reported p-values were calculated based on these permuted datasets using Mann-Whitney U tests. To address the question whether toxic si/shRNAs target survival genes or all genes that are highly expressed, we recalculated the TI based on a set of 850 highly expressed and expression matched survival and nonsurvival genes. The results were similar to the ones obtained with the original TI (data not shown). Our data suggests that it is possible to predict the experimental toxicity of shRNAs based on the *in silico* calculated TI to some extent.

CD95L mRNA is toxic to cancer cells.

Expression of CD95L in most cancer cells is known to kill them through induction of apoptosis. Consequently, expressing CD95L in HeyA8 cells, which are highly sensitive to CD95 mediated apoptosis, resulted in induction of apoptosis within a few hours of infecting the cells with a lentiviral CD95L (**Fig. 5a**, left panel). Severe growth reduction was seen without any signs of apoptosis (not shown) when a CD95L mutant was expressed carrying a Y218R point mutation (expressed at similar levels as wt CD95L, **Fig. 5b**) which prevents the CD95L protein to bind to CD95 (CD95L^{MUT} in **Fig. 5a**)³³. To prevent full length CD95L protein to be produced by the CD95L mRNA we also introduced a premature stop codon right after the start codon in the CD95L^{MUT} vector (CD95L^{MUT}NP). This construct (confirmed to produce mRNA with no detectable full length CD95L protein, **Fig. 5b**) was equally active in reducing the growth of HeyA8 cells when compared to the CD95L^{MUT} vector (**Fig. 5a**, left panel). This result suggested that the CD95L mRNA could be toxic to HeyA8 cells without inducing apoptosis. This was confirmed by expressing the three CD95L constructs in the presence of the caspase inhibitor zVAD-fmk (**Fig. 5a**, centre panel). Even with suppressed apoptosis all three constructs were equally toxic to HeyA8 cells. Finally, we tested three HeyA8 CD95 protein k.o. clones (**Fig. S3**). In these cells without the addition of zVAD-fmk, wt CD95L and CD95L^{MUT}NP were equally

active in severely reducing the growth of the cells (**Fig. 5a**, right panel and data not shown). These data suggested that it is the CD95L mRNA that killed the cells. Massive cell death could be seen in the CD95^{-/-} cells treated with CD95L. This cell death resembled DISE induced by shRNAs⁹ and cells showed the same inability to pass through mitosis without dying (**Movies S1-S4**). Cell death was confirmed by quantifying nuclear fragmentation (**Fig. 5c** bottom) and we also detected a significant increase in ROS in CD95L expressing cells (**Fig. 5c**, top) one of the main features of ongoing DISE⁹. To exclude the possibility that truncated CD95 protein or any part of the CD95 mRNA would play a role in this toxicity, we deleted the entire CD95 gene in MCF-7 cells (**Fig. S9**). Wt CD95L killed these complete CD95 knock-out cells as well as CD95 shR6 deletion cells (**Fig. S9f**). To determine the cause of cell death induced by CD95L mRNA in HeyA8 CD95^{-/-} cells, we performed an RNA Seq analysis. Similar to cells treated with CD95L derived si/shRNAs, we observed that downregulated genes were enriched in survival genes versus the nonsurvival control genes (**Fig. 5c**). In addition, cell death induced by CD95L mRNA resulted in a substantial loss of 11 of the 12 histones already detected to be downregulated in cells treated with sh/siRNAs (**Fig. 5d**). A Metascape analysis confirmed that nucleosome assembly, regulation of mitosis and genes that are consistent with the deacetylation of histones were among the most significantly downregulated RNAs across all cells in which DISE was induced by any of the four sh/siRNAs or by CD95L (**Fig. 5e**). These GO clusters are consistent with DISE being a form a mitotic catastrophe with cells unable to survive cell division⁹. Also, very similar to the death induced by CD95L derived shRNAs, Drosha^{-/-} cells were hypersensitive to the expression of CD95L^{MUT}NP (**Fig. 5f**) and now virtually all cells died (**Fig. 5g**). Taken together the data suggest that overexpression of CD95L mRNA and si/shRNAs derived from CD95L kill cancer cells by a related mechanism involving the RNAi machinery and targeting survival genes.

Discussion

Most of the current use of RNAi is aimed at achieving a highly specific silencing with little OTE. In fact, OTE represents one of the largest impediments to the use of RNAi in phenotypic screening applications. We now demonstrate that DISE is a unique form of OTE that results in the simultaneous activation of multiple cell death pathways in cancer cells. The discovery that DISE involves loss of multiple survival genes now provides an explanation for the unique properties we described for this form of cell death, especially the observation that cancer cells have a hard time developing resistance to this cell death mechanism^{9,34}.

Our data on DISE are consistent with a number of properties of RNAi OTE previously reported. Similar to DISE, OTE mediated silencing requires a 6/7nt seed sequence of complementarity¹⁹⁻²¹ and it targets mRNAs in the 3'UTR²⁰. While it has been shown that the TRC shRNAs used in our study can give rise to increased OTE³⁰, our data on siRNAs and DsiRNAs suggest that DISE is not limited to one platform and requires sequence specific targeting. This conclusion is also consistent with a previous report that suggested that sequence-dependent off-target transcript regulation is independent of the delivery method²¹. The authors found the same enrichment of 6mers and 7mers in 3'UTRs of targeted mRNAs for siRNAs and shRNAs²¹. The most compelling argument against an effect limited to si/shRNAs, however, is the discovery that the mRNA of CD95L, which we showed to be enriched in RNAi active toxic sequences, itself is toxic to cancer cells. Overexpression of CD95L mRNA in most cells will induce massive apoptosis and when it was discovered previously that CD95L delivered using viruses very efficiently killed multiple cancer cells that were completely resistant to CD95 mediated apoptosis, this was interpreted as a form of CD95L induced apoptosis that occurred from within the cells³⁵⁻³⁸. We now conclude that the mRNA of CD95L kills cells in the same way as CD95L-derived si/shRNAs based on the following observations: 1) The morphology of the cells undergoing DISE induced by shRNAs and by overexpressing CD95L is virtually identical (see supplementary movies). 2) Both treatments result in generation of ROS. 3) The kinetics of these two forms of cell death are similar (days rather than hours). 4) We detect large numbers of cells that die just after the first attempt to divide (data not shown). 5) *Drosha*^{-/-} and *Dicer*^{-/-} cells are hypersensitive to si- and or shRNAs and CD95L RNA mediated toxicity. 6) Both forms of cell death result in a preferential loss of critical survival genes followed by loss of histones. It was first shown in plants that overexpressed transgenes can be converted into RNAi active short RNA sequences in a process referred to as posttranscriptional gene silencing³⁹. Our data on the effects of overexpressed CD95L RNA maybe the first example of transgene determining cell fate through the RNAi mechanism in mammalian cells.

We interpret the hypersensitivity of both *Drosha*^{-/-} and *Dicer*^{-/-} cells to DISE in the following way: Most of the small RNAs in the cells that are loaded into the RISC are miRNAs. Using Ago pull-down experiments we determined ~99.3% of Ago associated RNAs in HeyA8 cells to be miRNAs (data not shown). It was recently reported that *Drosha*^{-/-} cells showed a reduction of miRNA content from roughly 70-80% to 5-6% and *Dicer*^{-/-} cells had a reduction down to 14-21%²⁵. Since neither *Drosha*^{-/-} nor *Dicer*^{-/-} cells express reduced Ago2 levels (see Fig. 2e) it is reasonable to assume that their RISC can take up many more of the toxic DISE inducing RNAs than the RISC in wt cells explaining the super toxicity of both DISE inducing si/shRNAs and CD95L mRNAs in these cells.

We previously showed that expression of either shL3 and shR6 induced DISE in immortalized normal ovarian fibroblasts much more efficiently than in matching nonimmortalized cells⁹, suggesting that this form of cell death preferentially affects transformed

cells. Our data now provide an interesting model to explain the higher sensitivity of cancer cells to DISE when compared to normal cells. It is well documented that cancer cells in general have global downregulation of miRNAs when compared to normal tissues⁴⁰. This might free up the RISC for DISE inducing RNAs and would imply that miRNAs may protect normal cells from DISE.

Overall our data allow us to predict that any small RNA with DISE inducing RNAi activity that does not require Dicer processing can kill cancer cells regardless of its Dicer or Drosha status. In fact, in an accompanying manuscript we demonstrate that DISE can be triggered *in vivo* to treat ovarian cancer in xenografted mice by delivering CD95L-derived siRNAs using nanoparticles³⁴. No toxicity was observed in the treated mice. Most interestingly, while cells *in vitro* and *in vivo* became resistant to treatment, they did not become resistant to the DISE mechanism itself but to the delivery of the sh- or siRNAs. These data suggest that it might be possible to develop a novel form of cancer therapy based on the DISE OTE mechanism.

Methods

Reagents and Antibodies. Primary antibodies for Western blot: anti- β -actin antibody (Santa Cruz #sc-47778), anti-human CD95L (BD Biosciences #556387), and anti-human CD95 (Santa Cruz #sc-715), anti-human Ago2 (Abcam #AB186733), anti-human Drosha (Cell Signaling #3364), and anti-Dicer (Cell Signaling #3363). Secondary antibodies for Western blot: Goat anti-rabbit; IgG-HRP (Southern Biotech #SB-4030-05 and Cell Signaling #7074), and Goat anti-mouse; IgG1-HRP; (Southern BioTech #1070-05). Antibodies/isotype controls for surface staining, S2 and leucine-zipper tagged (Lz)CD95L were described before⁴¹. Reagents used: propidium iodide (Sigma #P4864), puromycin (Sigma #P9620), G418 (Affymetrix #11379), zVAD-fmk (Sigma-Aldrich #V116, used at 20 μ M), and doxycycline (Sigma #9891).

Cell lines. The ovarian cancer cell line HeyA8, the neuroblastoma cell line NB7, and the breast cancer cell line MCF-7 were grown in RPMI 1640 medium (Cellgro #10-040-CM), 10% heat-inactivated FBS (Sigma-Aldrich), 1% L-glutamine (Mediatech Inc), and 1% penicillin/streptomycin (Mediatech Inc). The human embryonic kidney cell line 293T was cultured in DMEM (Cellgro #10-013-CM), 10% heat-inactivated FBS, 1% L-Glutamine, and 1% penicillin/streptomycin.

HCT116 parental, Drosha^{-/-}, and Dicer^{-/-} cells were generated by Narry Kim²⁵. HCT116 parental (cat#HC19023), a Drosha^{-/-} clone (clone #40, cat#HC19020) and two Dicer^{-/-} clones (clone #43, cat#HC19023 and clone #45, cat#HC19024) were purchased from Korean Collection for Type Cultures (KCTC). All HCT116 cells were cultured in McCoy's medium (ATCC, cat#30-2007), 10% heat-inactivated FBS, 1% L-Glutamine, and 1% penicillin/ streptomycin.

NB7 cells overexpressing wild type CD95L and mutant CD95L cDNAs were generated by seeding cells at 50,000 to 100,000 cells per well in a 6-well plate and infecting cells with lentivirus generated in 293T cells from the pLenti-CD95L, pLenti-CD95L1MUT, pLenti-CD95L3MUT, pLenti-CD95L^{MUT}, and pLenti-CD95L^{MUT}NP vectors in the presence of 8 μ g/ml polybrene. Selection was done with 3 μ g/ml puromycin 48 hours after infection. HCT116 and HCT116 Drosha^{-/-} cells overexpressing CD95L^{MUT}NP were generated by seeding cells at 100,000 cells per well in a 24-well plate and infecting cells with lentivirus generated in 293T cells from the pLenti-CD95L^{MUT}NP vector in the presence of 8 μ g/ml polybrene. Selection was done with 3 μ g/ml puromycin 48 hours after infection. Both HeyA8 cells and HCT116 cells overexpressing CD95L were plated in 96-well plate for incuCyte analysis one day after selection in the presence of puromycin. MCF-7 cells overexpressing CD95 cDNAs were generated by seeding cells at 50,000 per well in a 6-well plate followed by infection with retrovirus generated in phoenix amphi 293 cells from the pLNCX2-CD95 or pLNCX2-CD95R6MUT vectors in the presence of 8 μ g/ml polybrene. Selection was done with 200 μ g/ml G418 48 hours after infection for 2 weeks. The HeyA8 cells used in Fig. 2d carried a lentiviral Venus-siL3 sensor vector³⁴ and were infected with NucLight Red lentivirus (Essen Bioscience #4476) with 8 μ g/ml polybrene and selected with 3 μ g/ml puromycin and sorted for high Venus expression 48 hours later. HeyA8 Δ shR6 clone #2 sensor cells used in Fig. 2a to c were infected with lentiviruses generated from the Venus-CD95L (full length) sensor vector to over-express the Venus-CD95L chimeric transcript. Cells were sorted for Venus expression 48 hours later.

Plasmids and constructs. The venus-CD95L ORF and venus-CD95 ORF (full length) sensor vectors were created by sub-cloning the Venus-CD95L or the Venus-CD95 inserts (synthesized

CCCATTTAACAGGCAAGTCCA), TRCN0000059000 (shL3:
ACTGGGCTGTACTTTGTATAT), TRCN0000059001 (shL4:
GCAGTGTTC AATCTTACCAGT), TRCN0000059002 (shL5:
CTGTGTCTCCTTGTGATGTTT), TRCN0000372231 (shL6:
TGAGCTCTCTCTGGTCAATTT), TRCN0000372232 (shL2': TAGCTCCTCAACTC
ACCTAAT), and TRCN0000372175 (shL5': GACTAGAGGCTTGCATAATAA), and 9 non-
overlapping shRNAs against human CD95 mRNA (accession number NM_000043),
TRCN0000218492 (shR2: CTATCATCCTCAAGGACATTA), TRCN0000038695 (shR5:
GTTGCTAGATTATCGTCCAAA), TRCN0000038696 (shR6: GTGCAGA
TGTAACCAAACTT), TRCN0000038697 (shR7: CCTGAAACAGTGGCAATAAAT),
TRCN0000038698 (shR8: GCAAAGAGGAAGGATCCAGAT), TRCN0000265627 (shR27':
TTTTACTGGGTACATTTTATC), TRCN0000255406 (shR6': CCCTTGTGTTT
GGAATTATAA), TRCN0000255407 (shR7': TTAAATTATAATGTTTGACTA), and
TRCN0000255408 (shR8': ATATCTTTGAAAGTTTGTATT). Infection was carried out
according to the manufacturer's protocol. In brief, 0.5 to 1 x 10⁵ cells seeded the day before in a
6-well plate were infected with each lentivirus at an M.O.I of 3 in the presence of 8 µg/ml
polybrene overnight. Media change was done the next day, followed by selection with 3 µg/ml
puromycin 24 hours later. Selection was done for at least 48 hours until puromycin killed the
non-infected control cells. For infection of NB7 cells over-expressing pLenti-CD95L with pLKO
lentiviral particles, cells were seeded at 5,000 per well on a 24-well plate and infected with an
M.O.I. of 20 to ensure complete infection. For infection of MCF-7 cells over-expressing
pLNCX2-CD95 with pLKO lentiviruses, cells were seeded at 7,000 per well on a 24-well plate
and infected at an M.O.I. of three. 3 µg/ml puromycin was added 48 hours after infection. For
infection of HCT116, Drosha^{-/-}, and Dicer^{-/-} cells, cells were seeded at 100,000 per well in a 24-
well plate and infected at an M.O.I of three. 3 µg/ml puromycin was added 48 hours after
infection.

Knockdown with pTIP-shRNA viruses. Cells were plated at 50,000 to 100,000 cells per well
in a 6-well plate. Cells were infected with lentivirus generated in 293T cells from the desired
pTIP-shRNA vector in the presence of 8 µg/ml polybrene. Media was replaced 24 hours later.
Selection was done 48 hours after infection with 3 µg/ml puromycin. Induction of shRNA
expression was achieved by adding 100 ng/ml doxycycline (Dox) to the media.

Transfection with short oligonucleotides. siRNAs were either purchased from Dharmacon
(Figs 3e-g and S5b and c, and S6b) or synthesized by IDT (Figs 1i, 2, and S1) as sense and
antisense RNA (or DNA for Fig 2b) oligos and annealed. The sense RNA oligonucleotides had 3'
2 deoxy-T overhangs. The antisense RNA oligos were phosphorylated at the 5' end and had 3'
2 deoxy-A overhangs. siRNAs targeting CD95L (and controls) were as follows: siRNA (Scr,
sense: UGGUUUACAUGUUGUGUGA), siL1 (sense: UACCAGUGCUGAUCAUUUA), siL2
(sense: CAACGUAUCUGAGCUCUCU), siL3 (sense: GCCCUUCAAUUACCCAUAU), siL4
(sense: GGAAAGUGGCCCAUUUAAC), and siL3MUT (sense:
GGACUUCAACUAGACAUCU). The siL3 DNA oligos (sense:
GCCCTTCAATTACCCATAT) and Scr DNA oligos (sense: TGGTTTACATGTTGTGTGA)
were used for the experiment in Fig. 2b. Blunt siL3 and Scr RNA oligos without the
deoxynucleotide overhangs as well as siL2 and siL3 RNA oligos with Cy5-labelled 5' or 3' ends
were used in the experiment in Fig. 2c. DsiRNA used in Fig. S1 were Dsi13.X (sense RNA
oligo: CAGGACUGAG AAGAAGUAAAACcdGdT, antisense RNA oligo:
ACGGUUUUACUUCUUCUCAGUCCUGUA), DsiL3 (sense RNA oligo:

CAGCCCUUCAAUUACCCAUAUCCdCdC, antisense RNA oligo:
GGGGAUAUGGGUAAUUGAAGGGCUCU), Dsi-13.2 (sense RNA oligo: AUCUU
ACCAGUGCUGAUCAUUUAdTdA, antisense RNA oligo:
UAUAAAUGAUCAGCACUGGUAAGAUUG), Dsi-13.3 (sense RNA oligo:
AAAGUAUACUCCGGGGUCAAUcTdT, antisense RNA oligo:
AAGAUUGACCCCGGAAGUAUACUUUGG), Dsi-13.9 (sense RNA oligo:
CUUCCGGGGUCAAUUCUUGCAACAdAdC, antisense RNA oligo: GUUGUUGC
AAGAUUGACCCCGGAAGUA), and a non-targeting DsiRNA control Dsi-NC1 (Sense:5'-
CGUUAUCGCGUAUAAUACGCGUdAdT, antisense:5'-
AUACGCGUAUUUACGCGAUUAACGAC, IDT #51-01-14-03). Predesigned siRNA
SmartPools targeting the 11 downregulated genes were obtained from Dharmacon and used in
Fig. 3c and Fig. S5b. Each siRNA SmartPool consisted of 4 siRNAs with On-Target^{plus}
modification. The following SmartPools were used: L-014208-02 (NUCKS1); L-012212-00
(CAPZA1); L-018339-00 (CCT3); L-013615-00 (FSTL1); L-011548-00 (FUBP1); L-017242-00
(GNB1); L-014597-01 (NAA50); L-020893-01 (PRELID3B); L-019719-02 (SNRPE); L-
003941-00 (TFRC); L-006630-00 (HIST1H1C). On-Target^{plus} non-targeting control pool (D-
001810-10) was used as negative control. HeyA8 cells were seeded at 750 cells per well on a 96-
well plate one day before transfection. Cells were transfected using 0.1 µl of Lipofectamine
RNAiMAX reagent (ThermoFisher Scientific #13778030) per well. HCT116 cells were seeded
at 4000 cells per well on a 96-well plate one day before transfection. 0.2 µl of Lipofectamine
RNAiMAX was used for transfection. Media was changed the day after transfection.

Soluble CD95L protein rescue experiments. NB7 cells were seeded at 500 cells per well in a
96-well plate. Next day, cells were infected with the scrambled pLKO lentiviruses or pLKO-
shL1 lentiviruses at an M.O.I. of 50 (to achieve 100% transduction efficiency under conditions
omitting the puromycin selection step) in the presence of 8 µg/ml polybrene and 100 ng/ml of S2
CD95L for 16 hrs. Media was replaced the next day with media containing varying
concentrations of recombinant S2 CD95L (50 ng/ml and 100 ng/ml). Cell confluence was
measured over time in the IncuCyte Zoom.

Real-time PCR. Total RNA was extracted and purified using QIAzol Lysis reagent
(QIAGEN) and the miRNeasy kit (QIAGEN). 200 ng of total RNA was used to generate cDNA
using the High-Capacity cDNA reverse Transcription kit (Applied Biosystems #4368814).
cDNA was quantified using Taqman Gene expression master mix (ThermoFisher Scientific
#4369016) with specific primers from ThermoFisher Scientific for GAPDH (Hs00266705_g1),
human CD95 (custom probe, Fr primer: *GGCTAACCCCACTCTATGAATCAAT*, Rev primer:
GGCCTGCCTGTTCACTAAGT, Probe: *CCTTTTGCTGAAATATC*), human CD95L
(Hs00181226_g1 and Hs00181225_m1), the shL3 target site in CD95L (custom probe, Fr
primer: *GGTGGCCTTGTGATCAATGAAA*, Rev primer: *GCAAGATTGACCCCGGAAG TATA*,
Probe: *CTGGGCTGTACTTTGTATATT*), and downstream of the shL3 site (custom probe, Fr
primer: *CCCAGGATCTGGTGATGATG*, Rev primer: *ACTGCCCCCAGGTAGCT*, Probe:
CCCACATCTGCCAGTAGT).

To perform arrayed real-time PCR (Fig S4), total RNA was extracted and used to make
cDNA as described for standard real-time PCR. For Taqman Low Density Array (TLDA)
profiling, custom-designed 384-well TLDA cards (Applied Biosystems #43422489) were used
and processed according to the manufacturer's instructions. Briefly, 50 µl cDNA from each
sample (200 ng total input RNA) was combined with 50 µl TaqMan Universal PCR Master Mix
(Applied Biosystems) and hence a total volume of 100 µl of each sample was loaded into each of

the 8 sample loading ports on the TLDA cards that were preloaded with assays from ThermoFisher Scientific for human GAPDH control (Hs99999905_m1) and for detection of ATP13A3 (Hs00225950_m1), CAPZA1 (Hs00855355_g1), CCT3 (Hs00195623_m1), FSTL1 (Hs00907496_m1), FUPB1 (Hs00900762_m1), GNB1 (Hs00929799_m1), HISTH1C (Hs00271185_s1), NAA50 (Hs00363889_m1), NUCKS1 (Hs01068059_g1), PRELID3B (Hs00429845_m1), SNRPE (Hs01635040_s1), and TFRC (Hs00951083_m1) after the cards reached room temperature. The PCR reactions were performed using Quantstudio 7 (ThermoFisher Scientific). Since each of the port loads each sample in duplicates on the TLDA card and because two biological replicates of each sample were loaded onto two separate ports, quadruplicate Ct values were obtained for each sample. Statistical analysis was performed using Student's t test. To prepare RNAs from CD95L overexpressing cells HeyA8 Δ shR6 clone #11 cells were plated at 75,000 cells per well in six-well plates and were infected with lentivirus generated in 293T cells from the pLenti-CD95L vector in the presence of 8 μ g/ml polybrene. Selection was done with 3 μ g/ml puromycin 48 hours after infection. Cells were plated at 600,000 per 15 mm dish (Greiner CELLSTAR, cat#P7237, Sigma) after one day of puromycin selection. Total RNA was harvested at 50 hours after plating for RNAseq analysis

Western blot analysis. Protein extracts were collected by lysing cells with RIPA lysis buffer (1% SDS, 1% Triton X-100, 1% deoxycholic acid). Protein concentration was quantified using the DC Protein Assay kit (Bio-Rad). 30 μ g of protein were resolved on 12% SDS-PAGE gels and transferred to nitrocellulose membranes (Protran, Whatman) overnight at 25 mA. Membranes were incubated with blocking buffer (5% non-fat milk in 0.1% TBS/Tween-20) for 1 hour at room temperature. Membranes were then incubated with the primary antibody diluted in blocking buffer over night at 4°C. Membranes were washed 3 times with 0.1% TBS/Tween-20. Secondary antibodies were diluted in blocking buffer and applied to membranes for 1 hour at room temperature. After 3 more additional washes, detection was performed using the ECL reagent (Amersham Pharmacia Biotech) and visualized with the chemiluminescence imager G:BOX Chemi XT4 (Synoptics).

CD95 surface staining. A pellet of about 300,000 cells was resuspended in 2% BSA/PBS on ice. Cells were resuspended with either anti-APO-1 primary antibody or the IgG3 isotype control diluted to 10 μ g/ml in 2% BSA/PBS. Cells were incubated on ice at 4°C for 30 minutes, washed with 2% BSA/PBS, and anti-IgG3-RPE was added diluted in 2% BSA/PBS. After an incubation for 30 minutes at 4°C, percent red cells were determined by flow cytometry (Beckman Coulter).

Cell death quantification (DNA fragmentation) and ROS production. A cell pellet (500,000 cells) was resuspended in 0.1% sodium citrate, pH 7.4, 0.05% Triton X-100, and 50 μ g/ml propidium iodide. After resuspension, cells were incubated 2 to 4 hours in the dark at 4°C. The percent of subG1 nuclei (fragmented DNA) was determined by flow cytometry. For pLKO shRNA infection experiments, subG1 quantification was performed eight days after infection. For siRNA and DsiRNA transfection experiments, subG1 quantification was performed four days after transfection. ROS production was quantified as previously described⁹.

Cell growth and fluorescence over time. After treatment/infection, cells were seeded at 700 to 1,500 per well in a 96-well plate in triplicate. Images were captured at indicated time points using an InCuCyte ZOOM live cell imaging system (Essen BioScience) with a 10x objective lens. Percent confluence, red object count, and the green object integrated intensity were calculated using the InCuCyte ZOOM software (version 2015A).

RNA-Seq analysis. HeyA8 Δ shR6 clone #11 was infected with pLKO-shScr or pLKO-shR6. A pool of three 293T Δ shL3 clones was infected with either pTIP-shScr or pTIP-shL3. After selection with puromycin, the pTIP-infected 293T cells were plated with Dox in duplicate at 500,000 cells per T175 flask. The pLKO-infected HeyA8 cells were plated at 500,000 cells per flask. Total RNA was harvested 50 hours and 100 hours after plating. RNA libraries were generated and sequenced (Genomics Core facility at the University of Chicago). The quality and quantity of the RNA samples was checked using an Agilent bio-analyser. Paired end RNA-SEQ libraries were generated using Illumina TruSEQ TotalRNA kits using the Illumina provided protocol (including a RiboZero rRNA removal step). Small RNA-SEQ libraries were generated using Illumina small RNA SEQ kits using the Illumina provided protocol. Two small RNA-SEQ sub-libraries were generated: one containing library fragments 140-150 bp in size and one containing library fragments 150-200 bp in size (both including the sequencing adaptor of about 130bp). All three libraries (one RNA-SEQ and two small RNA-SEQ) were sequenced on an Illumina HiSEQ4000 using Illumina provided reagents and protocols. The raw counts for RNAs were calculated by HTSeq. The sequenced reads were mapped to hg38 human genome using Tophat and bowtie2. Differential gene expression was analysed by R Bioconductor DESeq2 package using shrinkage estimation for dispersions and fold changes to improve stability and interpretability of estimates. P values and adj P values were calculated using the DESeq2 package. Counts and sequences of small RNAs were extracted from raw fastq file by UNIX shell scripts and then grouped and summarized by SQL language in database tables. To extract small RNAs (shRNA sequences) adaptor sequences were removed using Trim Galore software.

In order to identify differentially abundant RNAs using a method unbiased by genome annotation, we also analysed the raw 100 bp reads for differential abundance. First, the second end in each paired end read was reverse complemented, so that both reads were on the same strand. Reads were then sorted and counted using the core UNIX utilities sort and uniq. Reads with fewer than 128 counts across all 16 samples were discarded. A table with all of the remaining reads was then compiled, summing counts from each sequence file corresponding to the same sample. This table contained a little over 100,000 reads. The R package edgeR (<http://bioinformatics.oxfordjournals.org/content/26/1/139>) was used to identify differentially abundant reads, and then these reads were mapped to the human genome using blat (<http://genome.cshlp.org/content/12/4/656.abstract>) to determine chromosomal location whenever possible. Homer (<http://homer.salk.edu/homer/>) was used to annotate chromosomal locations with overlapping genomic elements (such as genes). Raw read counts in each sequence file were normalized by the total number of unique reads in the file.

To identify the most significant changes in expression of RNAs both methods of RNAs Seq analysis (alignment and read based) were used to reach high stringency. All samples were prepared in duplicate and for each RNA the average of the two duplicate was used for further analysis. In the alignment based analysis only RNAs were considered that had a base mean of >2000 reads and were significantly deregulated between the groups (adjusted p-value <0.05). Only RNAs were scored as deregulated when they were more than 1.5 fold changed in the shL3 expressing cells at both time points and in the shR6 expressing cells at either time points (each compared to shScr expressing cells) (Table S1). This was done because we found that the pLKO driven expression of shR6 was a lot lower than the pTIP driven expression of shL3 (see the quantification of the two shRNAs in Fig. S6a) and likely as a result of the cell responses in the shR6 expressing cells were reduced. In the read based analysis only normalized read numbers of >10 across the samples in each treatment were considered. Only RNA reads were further considered that had a variation between duplicates of less than 2 fold. Only RNAs reads were

(CustomArray Inc, Custom 12K oligo pool). Each shRNA pool had its own unique 5' end represented by the poly-*X* region. This allowed selective amplification of a particular pool using 1 of 5 unique Fr primers (CD95L ORF: 5'-*TGGCTTTATATATCTCCCTATCAGTG*-3', CD95L 3' UTR: 5'-*GGTCGTCCT ATCTATTATTATTCACG*-3', CD95 ORF: 5'-*TCTTGTGTCCAGACCAATTTATTTTCG*-3', CD95 3'UTR: 5'-*CTCATTGACTATCGTTTTAGCTACTG*-3', Venus: 5'-*TATCATCTTTCATGATGACTTTCGGG*-3') and the common reverse primer 5'-*AATCAATGTCAACGCAGCAT*-3'. Phusion High Fidelity Polymerase was used to amplify each library pool; standard PCR conditions were used with an annealing temperature of 61°C and 15 cycles. PCR reactions were purified using PCR Cleanup kit (QIAGEN). The pTIP-shR6 vector and each of the amplified libraries were digested with SphI-HF and BsaBI. Digested PCR products were run on either a 2% Agarose gel or a 20% polyacrylamide (29:1) gel made with 0.5 x TBE buffer. PCR products were extracted using either Gel Extraction kit (QIAGEN) for extraction from Agarose gels or via electro-elution using D-Tube Dialyzer Mini columns (Novagen #71504). Purified PCR inserts were then ligated to the linearized pTIP vector with T4 DNA ligase for 24 hours at 16°C. The ligation mixtures were transformed via electroporation in MegaX DH10B T1 cells (Invitrogen #C6400) and plated on 24 cm ampicillin dishes. At least 10 colonies per pool were picked and sequenced to verify successful library construction. After verification, all colonies per library were pooled together and plasmid DNA extracted using the MaxiPrep kit (QIAGEN). The 5 pTIP-shRNA library DNA preps were used to produce virus in 293T cells.

Lethality screen with pTIP-shRNA libraries. NB7 cells were seeded at 1.5×10^6 per 145 cm² dish. Two dishes were infected with each of the 5 libraries with a transduction efficiency of about 10 to 20%. Media was replaced next day. Infected cells were selected with 1.5 µg/ml puromycin. Cells infected with the Venus, CD95L ORF, and CD95L 3'UTR-targeting libraries were pooled in a 1:1:1 ratio to make the CD95L cell pool. Likewise, cells infected with the Venus, CD95 ORF, and CD95 3'UTR-targeting libraries were pooled to make the CD95 receptor cell pool. The CD95 and the CD95L cell pools were plated separately each in 2 sets of duplicates seeded at 600,000 cells per 145cm² dish. One set received 100 ng/ml Dox, and the other one was left untreated (total of 4 dishes per combined pool; 2 received no treatment and 2 received Dox). Cells infected with the different libraries were also plated individually in triplicate with or without Dox on a 96-well plate to assess the overall toxicity of each pool. DNA was collected from each 145cm² dish 9 days after Dox addition.

The shRNA barcodes were amplified from the harvested DNA template using NEB Phusion Polymerase with 4 different pairs of primers (referred to as N, N+1, N+2, and N+3) in separate reactions per DNA sample. The N pair consisted of the primers used to amplify the CD95L ORF library (Fr: 5'-*TGGCTTTATATATCTCCCTATCAGTG*-3' and Rev: 5'-*AATCAATGTCAACGCAGCAT*-3'). The N+1 primers had a single nucleotide extension at each 5' end of the N primers corresponding to the pTIP vector sequence (Fr: 5'-*TTGGCTTTATATATCTCCCTATCAGTG*-3' and Rev: 5'-*TAATCAATGTCAACGCAGCAT*-3'). The N+2 primers had 2 nucleotide extensions (Fr: 5'-*CTTGGCTTTATATATCTCCCTATCAGTG*-3' and Rev: 5'-*ATAATCAATGTCAACGCAGCAT*-3'), and the N+3 primers had 3 nucleotide extensions (Fr: 5'-*TCTTGGCTTTATATATCTCCCTATCAGTG*-3' and Rev: 5'-*ATAATCAATGTCAACGCAGCAT*-3'). The barcodes from the pTIP-shRNA library plasmid preparations were also amplified using Phusion Polymerase with the N, N+1, N+2, and N+3 primer pairs. The shRNA barcode PCR products were purified from a 2% Agarose gel and submitted for 100 bp paired-end deep sequencing (Genomics Core facility at the University of Chicago). DNA was quantitated using

the Qubit. The 4 separate PCR products amplified using N, N+1, N+2, and N+3 were combined in equimolar amounts for each sample. Libraries were generated using the Illumina TruSeq PCR-free kit using the Illumina provided protocol. The libraries were sequenced using the HiSeq4000 with Illumina provided reagents and protocols. Raw sequence counts for DNAs were calculated by HTSeq. shRNA sequences in the PCR pieces of genomic DNA were identified by searching all reads for the sense sequence of the mature shRNA plus the loop sequence CTCGAG. To avoid a division by zero problem during the subsequent analyses all counts of zero in the raw data were replaced with 1. A few sequences with a total read number <10 across all plasmids reads were not further considered. In the CD95L pool this was only one shRNA (out of 2362 shRNAs) (L792') and in the CD95 20 shRNAs (out of 3004 shRNAs) were not represented (R88, R295, R493, R494, R496, R497, R498, R499, R213', R215', R216', R217', R220', R221', R222', R223', R225', R226', R258', R946', R1197', R423'). While most shRNAs in both pools had a unique sequence two sequences occurred 6 times (L605', L607', L609', L611', L613', L615', and L604', L606', L608', L610', L612', L614'). In these cases read counts were divided by 6. Two shRNAs could not be evaluated: 1) shR6 in the CD95 pool. It had a significant background due to the fact that the pTIP-shR6 was used as a starting point to clone all other shRNAs. 2) shL3 was found to be a minor but significant contaminant during the infection of some of the samples. For each condition two technical duplicates and two biological duplicates were available. To normalize reads in order to determine the change in relative representation of shRNAs between conditions, the counts of each shRNA in a subpool (all replicates and all conditions) was divided by the total number of shRNAs in each subpool (%). First, the mean of the technical replicates (R1 and R2) was taken. To analyse the biological replicates and to determine the changes between conditions, two analyses were performed: 1) The change in shRNA representation between the cloned plasmid library and cells infected with the library and then cultured for 9 days without Dox (infection -Dox). Fold downregulation was calculated for each subpool as $[(\text{plasmid } \%/ -\text{Dox1 } \% + \text{plasmid } \%/ -\text{Dox2 } \%)/2]$. 2) The difference in shRNA composition between the infected cells cultured with (infection +Dox) and without Dox. Fold downregulation was calculated for each subpool as $[(-\text{Dox1 } \%/ + \text{Dox1 } \%)/(-\text{Dox1 } \%/ + \text{Dox2 } \%)/(-\text{Dox2 } \%/ + \text{Dox1 } \%)/(-\text{Dox2 } \%/ + \text{Dox2 } \%)/4]$. Only shRNAs were considered that were at least 5 fold underrepresented in either of the two analyses (data in Table S3).

The toxicity index (TI). The TI is defined by the sum of the counts of a 6mer or 8mer seed match in the 3'UTRs of critical survival genes divided by the seed match counts in the 3'UTRs of nonsurvival genes. We used the 1882 survival genes recently described in a CRISPR/Cas9 lethality screen by Wang et al.¹⁰. The survival genes were defined by having a CRISPR score of <-0.1 and an adjusted p-value of <0.05. We chose as a control group to these top essential genes the bottom essential genes using inverse criteria (CRISPR score of >0.1 and adjusted p-value of <0.05) and are referring to them as the "nonsurvival genes". Both counts were normalized for the numbers of genes in each gene set. 3'UTRs were retrieved as described above. For the survival genes 1846 and for the nonsurvival genes 416 3'UTRs were found. For each gene only seed matches in the longest 3'UTR were counted. The TI was calculated for each of the 4096 possible 6mer combinations and each of the 65536 possible 8mer combinations (Table S4). These numbers were then assigned to the results of the shRNA screen (Table S5).

Sylamer analysis. Sylamer is a tool to test for the presence of RNAi-type regulation effects from a list of differentially expressed genes, independently from small RNA measurements²⁸ (<http://www.ebi.ac.uk/research/enright/software/sylamer>). For short stretches of RNA (in this case length 6, 7, and 8 in length corresponding to the lengths of the determinants of seed region

binding in RNAi-type binding events), Sylamer tests for all possible motifs of this length whether the motif occurrences are shifted in sequences associated with the list under consideration, typically 3'UTRs when analysing RNAi-type binding events. A shift or enrichment of such a motif towards the down-regulated end of the gene list is consistent with upregulation of a small RNA that has the motif as the seed region. Sylamer tests in small increments along the list of genes, using a hypergeometric test on the counts of a given word, comparing the leading part of the gene list to the universe of all genes in the list. For full details refer to ²⁸. Enriched motifs stand out from the back-ground of all motifs tested, as visible in the Sylamer plot. The plot consist of many different lines, each line representing the outcomes of a series of tests for a single word, performed along regularly spaced intervals (increments of 200 genes) of the gene list. Each test yields the log-transformed P-value arising from a hypergeometric test as indicated above. If the word is enriched in the leading interval the log-transformed value has its value plotted on the positive y-axis (sign changed), if the word is depleted the log-transformed value is plotted on the negative y-axis. 3' UTRs were used from Ensembl, version 76. As required by Sylamer, they were cleaned of low-complexity sequences and repetitive fragments using respectively Dust ⁴⁴ with default parameters and the RSAT interface ⁴⁵ to the Vmatch program, also run with default parameters. Sylamer (version 12-342) was run with the markov correction parameter set to 4.

Statistical analyses. Continuous data were summarized as means and standard deviations and dichotomous data as proportions. Continuous data were compared using t-tests for two independent groups and one-way ANOVA for 3 or more groups. For evaluation of continuous outcomes over time, two-way ANOVA was used with one factor for the treatment conditions of primary interest and a second factor for time treated as a categorical variable to allow for non-linearity. Comparisons of single proportions to hypothesized null values were evaluated using binomial tests. Statistical tests of two independent proportions were used to compare dichotomous observations across groups. To test if higher TI is enriched in shRNAs that were highly downregulated, p-values were calculated based on permuted datasets using Mann-Whitney U tests. The ranking of TI was randomly shuffled 10,000 times and the W statistic from our dataset was compared to the distribution of the W statistic of the permuted datasets. Test of enrichment was based on the filtered data of at least 5-fold difference, which we define as a biologically meaningful. Fisher Exact Test was performed to assess enrichment of downregulated genes amongst genes with si/shRNA seed matches. All statistical analyses were conducted in Stata 14 or R 3.3.1.

Data availability. The accession numbers for the RNA-Seq and expression data reported in this paper are GSE87817 and GSE96620.

Acknowledgements

We are grateful to Lindsay Stolzenburg and Ann Harris for helping to set up the CRISPR/Cas9 gene editing method and to Denise Scholtens for biostatistics support. This work was funded by training grants T32CA070085 (to M.P.) and T32CA009560 (to W.P.) R50CA211271 (to J.C.Z.), and R35CA197450 (to M.E.P.).

Author contributions

W.P. planned the study and performed experiments. M.P. established the multiplex qPCR method and performed experiments, Q.Q.G., A.H., A.S.A.Q., A.S., A.H.K., and A.E.M. performed experiments, S.D. performed the SYMALER analysis, E.B. and J.S.Z. provided biocomputational and K.A.K. biostatistics support, M.H. provided assistance and discussions on the mechanism of RNAi and the RISC, and M.E.P. directed the study and wrote the manuscript.

Additional information

Supplementary Information accompanies this paper at

Figure legends

Figure 1. CD95 and CD95L derived si/shRNAs kill cells in the absence of the targeted site in CD95 or CD95L. (a) Schematic of the genomic locations and sequences of the gRNAs used to excise the siL3 ($\Delta 64$ bp) and shL3 ($\Delta 41$ bp) target sites from CD95L. PAM site is underlined. Green indicates a gRNA targeting the sense strand. Blue indicates a gRNA targeting the antisense strand. (b) Schematic showing the genomic locations and sequences of the gRNAs used to excise the shR6 ($\Delta 227$ bp) target site. (c) PCR with flanking (*top panels*) and internal (*bottom panels*) primers used to confirm the $\Delta 41$ deletion in the shL3 site in 293T clones. Cells transfected with Cas9 only (Cas9) are wild-type, clone #3 is heterozygous, and clones #1 and #5 carry homozygous deletions. (d) Quantitative PCR for endogenous CD95L with a primer downstream of the $\Delta 41$ shL3 deletion and another primer internal to the deleted region. nd, not detectable. (e) PCR with flanking (*top row*) and internal (*bottom row*) primers used to confirm the presence of the shL3 $\Delta 41$ (*top panel*), siL3 $\Delta 64$ (*middle panel*), and shR6 $\Delta 227$ (*bottom panel*) deletions in HeyA8 clones. Mix, HeyA8 cells after transfection with Cas9 and gRNAs but before single cell cloning. (f) Quantitative PCR for CD95 in HeyA8 cells transfected with Cas9 plasmid (Cas9) alone, or the HeyA8 Δ shR6 clone #11. RNA was extracted 5 days after infection with pLKO-shScr, pLKO-shR6, pLKO-shR2, or pLKO-shR6' (targeting the 3'UTR). (g) Percent cell confluence over time of 293T cells (*left*) and a pool of three 293T clones with a homozygous deletion of the shL3 target site (*right*) infected with pTIP-shScr or pTIP-shL3 and treatment with or without Dox. (h) *Left*: Percent confluence over time of HeyA8 cells infected with pLKO-shScr, pLKO-shR6, or pLKO-shL3. *Centre*: Percent confluence over time of a HeyA8 clone with a homozygous deletion of the shR6 target site infected with either pLKO-shScr or pLKO-shR6. *Right*: Percent confluence over time of a pool of three HeyA8 clones with a homozygous deletion of the shL3 site infected with either pLKO-shScr or pLKO-shL3. (i) Percent confluence over time of a pool of three HeyA8 clones harbouring a homozygous deletion of the siRNA L3 (siL3) target site after transfection with different concentrations of siScr or siL3.

Figure 2. Toxicity of CD95L derived siRNAs involves canonical RNAi activity. (a) Percent cell confluence (*left*) and total green object integrated intensity (*right*) over time of a HeyA8 CD95 knockout clone ($\Delta R6$ cl#2) expressing the Venus-CD95L sensor after transfection with 25 nM of single-stranded sense, single-stranded antisense, or double-stranded (ds) siScr or siL3 siRNAs. The CD95L sensor is schematically shown and comprises the Venus ORF fused to the CD95L ORF lacking the A of the ATG start codon (X). (b) Percent cell confluence (*left*) and total green object integrated intensity (*right*) over time of the HeyA8 CD95L sensor cell used in Fig. 2a after transfection with 5 nM siScr or siL3 double-stranded RNA (dsRNA) or double-stranded DNA (dsDNA). (c) Summary of experiments to test whether siL3 and siL2 siRNAs modified as indicated (*left*) were active (check mark) or not (X) in reducing green fluorescence or cell growth (both $>70\%$ reduction at end point) when transfected at 25 nM siRNAs (except for blunt end oligonucleotides which were used at 5 nM and compared to 5 nM of siL3) into HeyA8 CD95L sensor cells used in Fig. 2a. Endpoints were 164 hours for blunt end siRNA transfection, 180 hrs for modified siL3 and 144 hrs for modified siL2 siRNA transfections. (d) Red object count over time of HeyA8 cells (expressing NucRed) after transfection with different ratios of siL3 and mutant siL3 (siL3MUT). (e) Percent cell confluence over time of HCT116 parental (*left*) or Dicer^{-/-} (clone #43, another Dicer^{-/-} clone, #45, gave a similar result), or Drosha^{-/-} (*right*) cells after infection with either shScr, shL3 or shR6. Inserts show expression levels of Drosha/Dicer and Ago2 levels in the tested cells. (f) Western blot analysis of HCT116 wt, Dicer^{-/-} or Drosha^{-/-} cells 5 days after infection with either pLKO-shScr or pLKO-shR6. (g) Percent cell

confluence over time of HCT116 wt, Dicer^{-/-} and Drosha^{-/-} cells after transfection with 25 nM siScr or siL3. **(h)** Percent reduction in Venus expression (green) and in cell number (red object count (red)) over time of HeyA8 cells expressing the Venus-CD95L sensor and red nuclei after transfection with 5 nM of different chimeric siRNAs generated by substituting nucleotides in the toxic siL3 with the scrambled siRNA sequence beginning at either the seed match end (top) or the opposite end (bottom) of siL3 after 188 hours. The schematic in the middle shows the sequence of siL3 and the Scr siRNA (both sense and antisense strands). The 6mer seed sequence region of siL3 (positions 2 to 7) is highlighted in light blue. Nucleotides shared by siScr and siL3 are labelled in grey.

Figure 3. Toxic shRNAs derived from CD95 and CD95L target a network of critical survival genes. **(a)** Schematic of RNA-Seq work flow for total RNA sample prepared both before (50 hrs) and during (100 hrs) induction of DISE after expressing either shR6 or shL3 from different vector systems (i.e. pLKO-shR6 and pTIP-shL3) in different cells (HeyA8 shR6 Δ 227 cells and 293T shL3 Δ 41 cells). **(b)** One mRNA was up and 11 mRNAs were downregulated in the cells treated with toxic shL3 and shR6 as shown in Fig. 3a. mRNAs shown in red were found to be essential cancer survival genes in two CRISPR lethality screens. The number of essential genes was enriched from 6.6% of the tested genes^{10,26} to 54.5% in our study ($p=3 \times 10^{-6}$ according to binomial distribution). The number of shL3 and shR6 6mer seed sequences in the 3'UTRs is shown for each gene in the green and yellow ovals, respectively. **(c)** The level of growth inhibition observed in HeyA8 cells transfected with siRNA SmartPools (25 nM) individually targeting the listed survival genes. The seven genes are shown targeting of which significantly reduced cell growth compared to cells transfected with a siScr pool at 140 hrs (samples done in quadruplicate) with an ANOVA $p < 0.05$. **(d)** Sylamer plots for the list of genes in the shL3 experiment (top) and the shR6 experiment (bottom) ordered from down-regulated to up-regulated. The most highly enriched sequence is shown which in each case is the 8mer seed match of the introduced shRNA. The red line corresponds to a p-value threshold of 0.05 after Bonferroni correction for the number of words tested (65536). Bonferroni-adjusted p-values are shown. The unadjusted p-values are $1.58E-24$ and $1.35E-26$, respectively. **(e)** Gene set enrichment analysis for a group of 1846 survival genes (*top 4 panels*) and 416 nonsurvival genes (*bottom 4 panels*) identified in a genome-wide CRISPR lethality screen¹⁰ after introducing Dox-inducible shL3 in 293T Δ shL3 cells (*left-most panels*), shR6 in HeyA8 Δ shR6 cells (*centre-left panels*), shL1 in parental 293T cells (*centre-right panels*), and siL3 in HeyA8 cells (*right-most panels*). Scrambled sequences served as controls. p-values indicate the significance of enrichment. **(f)** Schematics showing all RNAs at least 1.5 fold downregulated (adj p-value < 0.05) in cells treated as in Fig. 3e. Of the histones only the ones underlined contain a 3'UTR. **(g)** A series of six 2x2 contingency tables comparing whether or not a gene is downregulated after treatment with the indicated siRNA or shRNA to whether or not its 3'-UTR contains at least 1 seed match for the introduced sh/siRNA. p-values were calculated using Fisher's Exact Test to determine any significant relationship between gene downregulation and presence of seed matches in 3'-UTR.

Figure 4. Identifying all toxic shRNAs derived from CD95L and CD95. **(a)** Schematic showing the cloned shRNAs covering the ORF of Venus and the ORFs and 3'UTRs of CD95L and CD95. The 3'UTR is displayed as a dashed line because it was not included in the full-length Venus-CD95L/CD95 sensors. **(b)** Work-flow of pTIP-shRNA library synthesis, shRNA screen and data analysis. **(c)** Ranked fold reduction of shRNAs spanning Venus and CD95L (ORF and 3'UTR) (*left 3 panels*) and Venus and CD95 (ORF and 3'UTR) (*right 3 panels*). The ranked lists

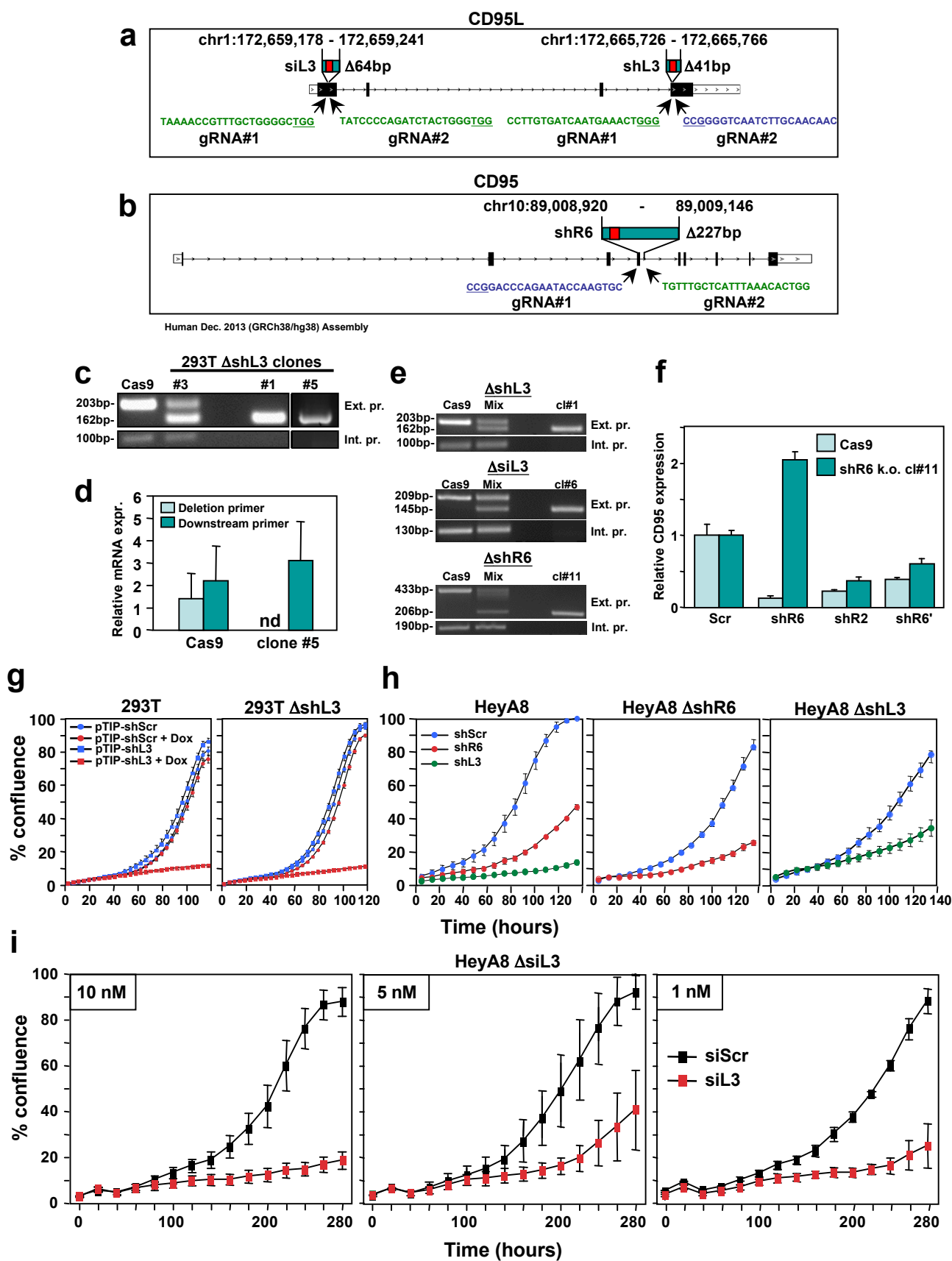
were separated into the shRNAs derived from Venus (top), the ORFs (centre) and the 3'UTRs (bottom). The p-value of enrichment for each ranked set of shRNAs is given. Only the parts of the ranked lists are shown with the downregulated shRNAs. For all 6 panels, the top section of each panel (boxed in blue) contains the data on shRNAs downregulated after infection of cells and cultured for 9 days without Dox when compared to the composition of the shRNA plasmid library and the bottom half (boxed in orange) contains the data on shRNAs downregulated after culture with Dox for 9 days when compared to the culture without Dox. P-values were calculated using Mann Whitney U tests with a one-sided alternative that the rank was lower. (d) The location of all shRNAs significantly downregulated at least 5 fold along the sequences of Venus, CD95L ORF, CD95L 3'UTR (left panel) and Venus, CD95 ORF, and CD95 3'UTR (right panel). The top half of each sub panel (blue ticks) shows the shRNAs downregulated after infection and the bottom half (orange ticks) contains the data on shRNAs downregulated after culture with Dox for 9 days. Significance of enrichment in the different subpanels is shown. p-values were calculated according to statistical tests of two proportions. Each data set was compared to the corresponding Venus distribution. (e) Fold downregulation versus ranked Toxicity Index for shRNAs of the Venus/CD95L pool (*left three panels*) and the Venus/CD95 pool (*right three panels*). Orange and blue tick marks indicate the same as in Fig. 4d. To test if higher TI is enriched in shRNAs that were highly downregulated, p-values were calculated based on permuted datasets using Mann-Whitney U tests. The ranking of TI was randomly shuffled 10,000 times and the W statistic from our dataset was compared to the distribution of the W statistic of the permuted datasets.

Figure 5. The CD95L RNA is toxic to cancer cells. (a) *Left*: the different CD95L mutants used. *Right*: Percent cell confluence over time of HeyA8 parental cells in the absence (*left panel*) or in the presence of zVAD-fmk (*centre panel*), or CD95^{-/-} cells (*right panel*; clone #11, see Fig. S3; similar results were obtained with clones 1 and 2 (data not shown)) after infection with lentiviral CD95L, CD95L^{MUT}, or CD95L^{MUT}NP. (b) *Left*: Western blot analysis of HeyA8 cells overexpressing different CD95L mutant RNAs. Cells expressing CD95L^{MUT} or CD95L were pretreated with zVAD. Note, the small amount of truncated CD95L in cells infected with CD95L^{MUT}NP does not have CD95 binding activity. *Right*: qPCR analysis for CD95L of the same samples. (c) Quantification of ROS production (top) and cell death (bottom) in cells expressing either pLenti (C) or pLenti-CD95L (L) at different time points.* p<0.05, ** p<0.001, *** p<0.0001. (d) Gene set enrichment analysis for the 1846 survival genes (*top panel*) and the 416 nonsurvival genes (*bottom panel*) of mRNAs downregulated in CD95L expressing HeyA8 CD95^{-/-} cells compared to parental HeyA8 cells. p-values indicate the significance of enrichment. (e) The genes downregulated in all cells after introduction of the four si/shRNAs derived from either CD95 or CD95L (see Fig. 3f). Histones underlined contain a 3'UTR. (f) Metascape analysis of 5 RNA Seq data sets analysed in Fig. 5d. The boxed GO term clusters were highly enriched in all 5 data sets. (g) Percent cell confluence over time of HCT116 parental (*left*) or Drosha^{-/-} (*right*) cells after infection with CD95^{MUT}NP. (h) Phase contrast images of Drosha^{-/-} cells 9 hours after infection with either empty vector or CD95L^{MUT}NP.

References

- 1 Krammer, P. H. CD95's deadly mission in the immune system. *Nature* **407**, 789-795 (2000).
- 2 Peter, M. E. *et al.* The CD95 receptor: apoptosis revisited. *Cell* **129**, 447-450 (2007).
- 3 Chen, L. *et al.* CD95 promotes tumour growth. *Nature* **465**, 492-496 (2010).
- 4 Barnhart, B. C. *et al.* CD95 ligand induces motility and invasiveness of apoptosis-resistant tumor cells. *EMBO J* **23**, 3175-3185 (2004).
- 5 Kleber, S. *et al.* Yes and PI3K Bind CD95 to Signal Invasion of Glioblastoma. *Cancer Cell* **13**, 235-248 (2008).
- 6 Ceppi, P. *et al.* CD95 and CD95L promote and protect cancer stem cells. *Nature Commun* **5**, 5238 (2014).
- 7 Drachsler, M. *et al.* CD95 maintains stem cell-like and non-classical EMT programs in primary human glioblastoma cells. *Cell Death Dis* **7**, e2209, doi:10.1038/cddis.2016.102 (2016).
- 8 Qadir, A. S. *et al.* CD95/Fas Increases Stemness in Cancer Cells by Inducing a STAT1-Dependent Type I Interferon Response. *Cell Rep* **18**, 2373-2386, doi:10.1016/j.celrep.2017.02.037 (2017).
- 9 Hadji, A. *et al.* Death induced by CD95 or CD95 ligand elimination. *Cell Reports* **10**, 208-222 (2014).
- 10 Wang, T. *et al.* Identification and characterization of essential genes in the human genome. *Science* **350**, 1096-1101, doi:10.1126/science.aac7041 (2015).
- 11 Hart, T., Brown, K. R., Sircoulomb, F., Rottapel, R. & Moffat, J. Measuring error rates in genomic perturbation screens: gold standards for human functional genomics. *Mol Syst Biol* **10**, 733, doi:10.15252/msb.20145216 (2014).
- 12 Morgens, D. W., Deans, R. M., Li, A. & Bassik, M. C. Systematic comparison of CRISPR/Cas9 and RNAi screens for essential genes. *Nat Biotechnol* **34**, 634-636, doi:10.1038/nbt.3567 (2016).
- 13 Krol, J., Loedige, I. & Filipowicz, W. The widespread regulation of microRNA biogenesis, function and decay. *Nat Rev Genet* **11**, 597-610 (2010).
- 14 Ha, M. & Kim, V. N. Regulation of microRNA biogenesis. *Nat Rev Mol Cell Biol* **15**, 509-524, doi:10.1038/nrm3838 (2014).
- 15 Zamore, P. D., Tuschl, T., Sharp, P. A. & Bartel, D. P. RNAi: double-stranded RNA directs the ATP-dependent cleavage of mRNA at 21 to 23 nucleotide intervals. *Cell* **101**, 25-33, doi:10.1016/S0092-8674(00)80620-0 (2000).
- 16 Siomi, H. & Siomi, M. C. On the road to reading the RNA-interference code. *Nature* **457**, 396-404, doi:10.1038/nature07754 (2009).
- 17 Pratt, A. J. & MacRae, I. J. The RNA-induced silencing complex: a versatile gene-silencing machine. *J Biol Chem* **284**, 17897-17901, doi:10.1074/jbc.R900012200 (2009).
- 18 Guo, H., Ingolia, N. T., Weissman, J. S. & Bartel, D. P. Mammalian microRNAs predominantly act to decrease target mRNA levels. *Nature* **466**, 835-840 (2010).
- 19 Lin, X. *et al.* siRNA-mediated off-target gene silencing triggered by a 7 nt complementation. *Nucleic Acids Res* **33**, 4527-4535, doi:10.1093/nar/gki762 (2005).
- 20 Birmingham, A. *et al.* 3' UTR seed matches, but not overall identity, are associated with RNAi off-targets. *Nat Methods* **3**, 199-204, doi:10.1038/nmeth854 (2006).
- 21 Jackson, A. L. *et al.* Widespread siRNA "off-target" transcript silencing mediated by seed region sequence complementarity. *RNA* **12**, 1179-1187, doi:10.1261/rna.25706 (2006).
- 22 Kim, D. H. *et al.* Synthetic dsRNA Dicer substrates enhance RNAi potency and efficacy. *Nat Biotechnol* **23**, 222-226, doi:10.1038/nbt1051 (2005).
- 23 Marques, J. T. & Williams, B. R. Activation of the mammalian immune system by siRNAs. *Nat Biotechnol* **23**, 1399-1405, doi:10.1038/nbt1161 (2005).

- 24 Grimm, D. *et al.* Fatality in mice due to oversaturation of cellular microRNA/short hairpin RNA pathways. *Nature* **441**, 537-541, doi:10.1038/nature04791 (2006).
- 25 Kim, Y. K., Kim, B. & Kim, V. N. Re-evaluation of the roles of DROSHA, Export in 5, and DICER in microRNA biogenesis. *Proc Natl Acad Sci U S A* **113**, E1881-1889, doi:10.1073/pnas.1602532113 (2016).
- 26 Blomen, V. A. *et al.* Gene essentiality and synthetic lethality in haploid human cells. *Science* **350**, 1092-1096, doi:10.1126/science.aac7557 (2015).
- 27 Hart, T. *et al.* High-Resolution CRISPR Screens Reveal Fitness Genes and Genotype-Specific Cancer Liabilities. *Cell* **163**, 1515-1526, doi:10.1016/j.cell.2015.11.015 (2015).
- 28 van Dongen, S., Abreu-Goodger, C. & Enright, A. J. Detecting microRNA binding and siRNA off-target effects from expression data. *Nat Methods* **5**, 1023-1025, doi:10.1038/nmeth.1267 (2008).
- 29 Khan, A. A. *et al.* Transfection of small RNAs globally perturbs gene regulation by endogenous microRNAs. *Nat Biotechnol* **27**, 549-555 (2009).
- 30 Gu, S. *et al.* The loop position of shRNAs and pre-miRNAs is critical for the accuracy of dicer processing in vivo. *Cell* **151**, 900-911, doi:10.1016/j.cell.2012.09.042 (2012).
- 31 Teitz, T. *et al.* Caspase 8 is deleted or silenced preferentially in childhood neuroblastomas with amplification of MYCN. *Nat Med* **6**, 529-535 (2000).
- 32 Pham, D. H., Moretti, P. A., Goodall, G. J. & Pitson, S. M. Attenuation of leakiness in doxycycline-inducible expression via incorporation of 3' AU-rich mRNA destabilizing elements. *Biotechniques* **45**, 155-156, doi:10.2144/000112896 (2008).
- 33 Schneider, P. *et al.* Characterization of Fas (Apo-1, CD95)-Fas ligand interaction. *J Biol Chem* **272**, 18827-18833 (1997).
- 34 Murmann, A. E. *et al.* Induction of DISE in ovarian cancer cells in vivo. *Oncotarget*, Accepted.
- 35 Sudarshan, S. *et al.* In vitro efficacy of Fas ligand gene therapy for the treatment of bladder cancer. *Cancer Gene Ther* **12**, 12-18, doi:10.1038/sj.cgt.7700746 (2005).
- 36 EIOjeimy, S. *et al.* FasL gene therapy: a new therapeutic modality for head and neck cancer. *Cancer Gene Ther* **13**, 739-745, doi:10.1038/sj.cgt.7700951 (2006).
- 37 Sun, H. *et al.* Efficient growth suppression and apoptosis in human laryngeal carcinoma cell line HEP-2 induced by an adeno-associated virus expressing human FAS ligand. *Head & neck* **34**, 1628-1633, doi:10.1002/hed.21985 (2012).
- 38 Hyer, M. L., Voelkel-Johnson, C., Rubinchik, S., Dong, J. & Norris, J. S. Intracellular Fas ligand expression causes Fas-mediated apoptosis in human prostate cancer cells resistant to monoclonal antibody-induced apoptosis. *Mol Ther* **2**, 348-358 (2000).
- 39 Hamilton, A. J. & Baulcombe, D. C. A species of small antisense RNA in posttranscriptional gene silencing in plants. *Science* **286**, 950-952 (1999).
- 40 Lu, J. *et al.* MicroRNA expression profiles classify human cancers. *Nature* **435**, 834-838 (2005).
- 41 Algeciras-Schimmich, A. *et al.* Two CD95 tumor classes with different sensitivities to antitumor drugs. *Proc Natl Acad Sci U S A* **100**, 11445-11450 (2003).
- 42 Mali, P. *et al.* RNA-guided human genome engineering via Cas9. *Science* **339**, 823-826, doi:10.1126/science.1232033 (2013).
- 43 Jinek, M. *et al.* RNA-programmed genome editing in human cells. *eLife* **2**, e00471, doi:10.7554/eLife.00471 (2013).
- 44 Morgulis, A., Gertz, E. M., Schaffer, A. A. & Agarwala, R. A fast and symmetric DUST implementation to mask low-complexity DNA sequences. *J Comput Biol* **13**, 1028-1040, doi:10.1089/cmb.2006.13.1028 (2006).
- 45 Medina-Rivera, A. *et al.* RSAT 2015: Regulatory Sequence Analysis Tools. *Nucleic Acids Res* **43**, W50-56, doi:10.1093/nar/gkv362 (2015).



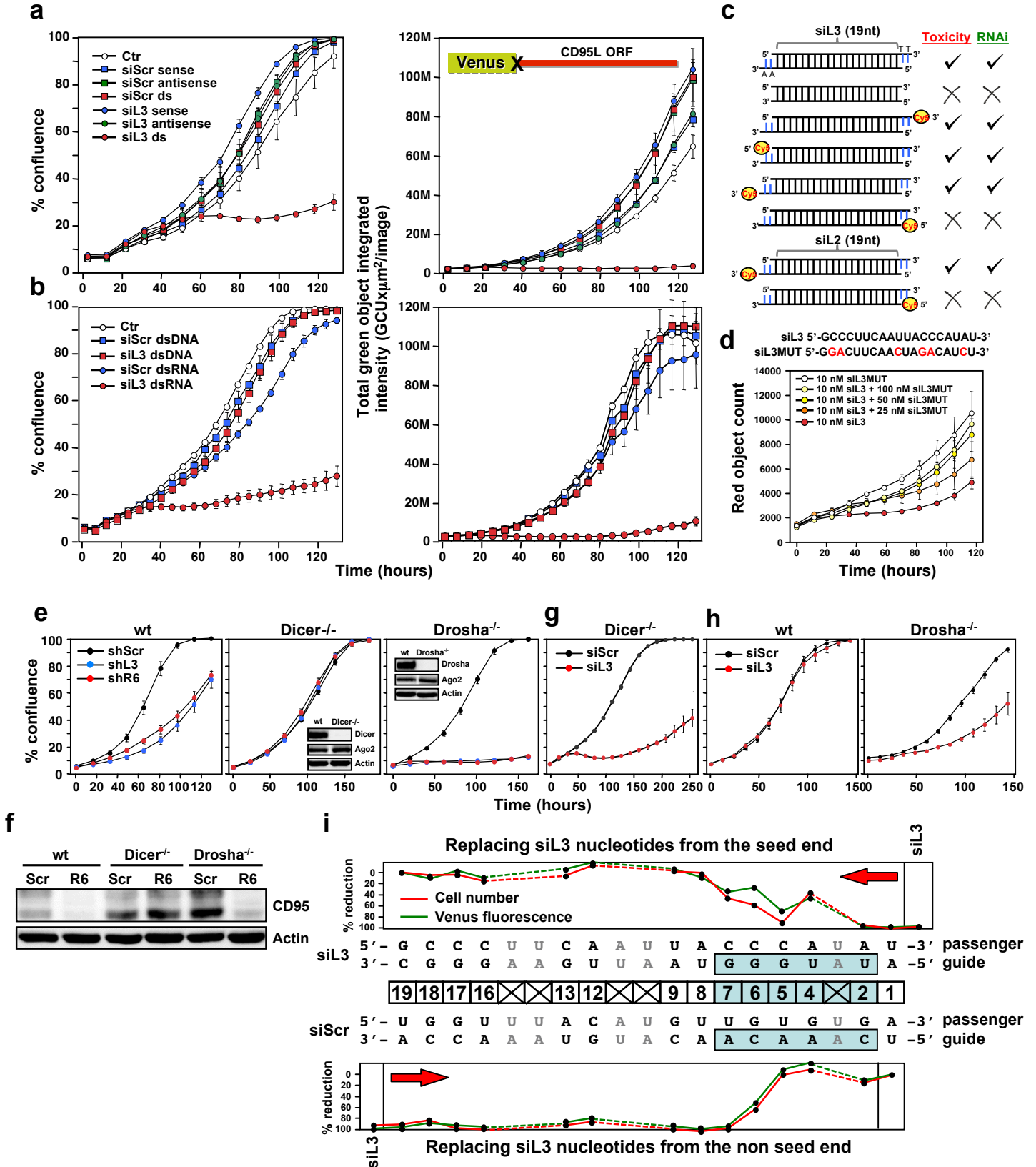
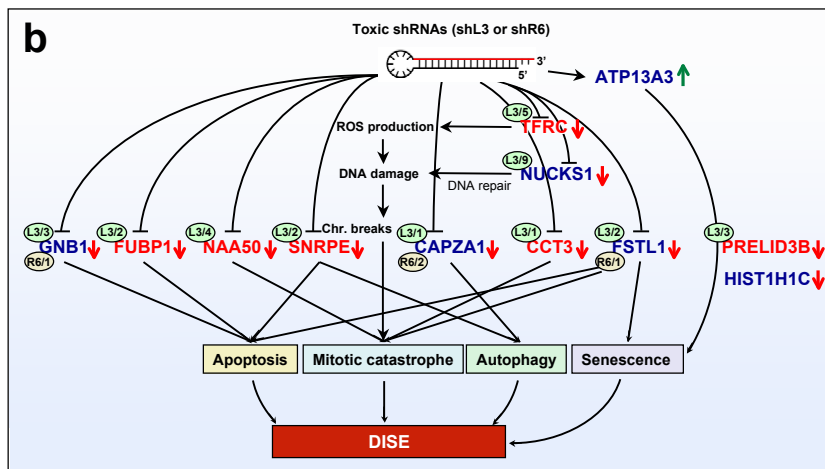
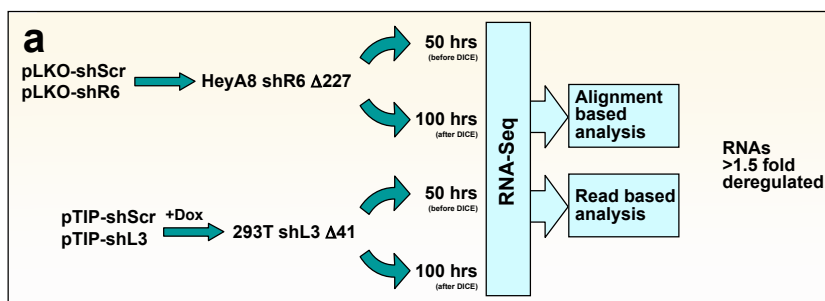
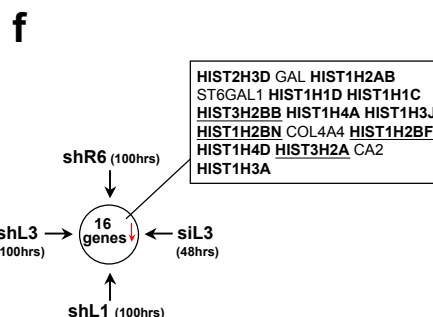
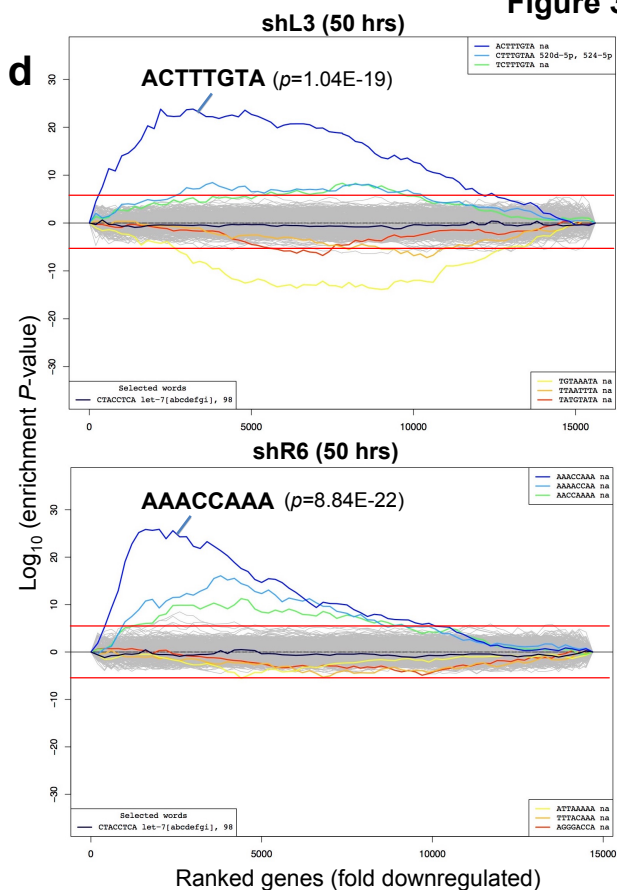
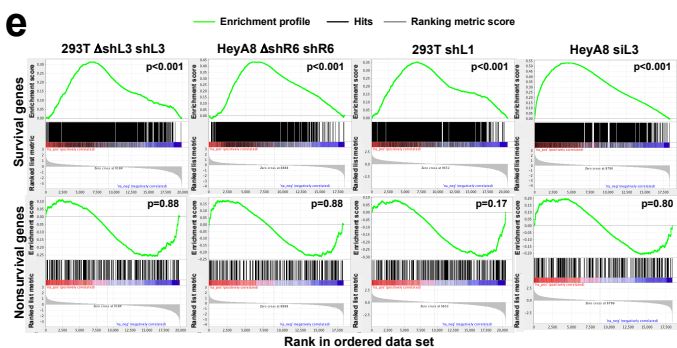


Figure 3



c

CCT3 (92.8%), TFRC (60.4%), NAA50 (44.7%), FUBP1 (19.7%), PRELID3B (16.0%), GNB1 (11.0%), FSTL1 (5.2%)



g

		No		Yes		No		Yes		No		Yes		No		Yes	
Seed match present	No	825	2	783	48	1113	13	1108	16	600	189	1205	238				
	Yes	904	55	850	109	612	40	619	31	746	259	244	93				
P-value		2.83E-13		2.58E-05		6.65E-09		4.31E-05		0.38		5.74E-06					
		shL3 (50hrs)		shL3 (100hrs)		shR6 (50hrs)		shR6 (100hrs)		shL1 (100hrs)		siL3 (48hrs)					

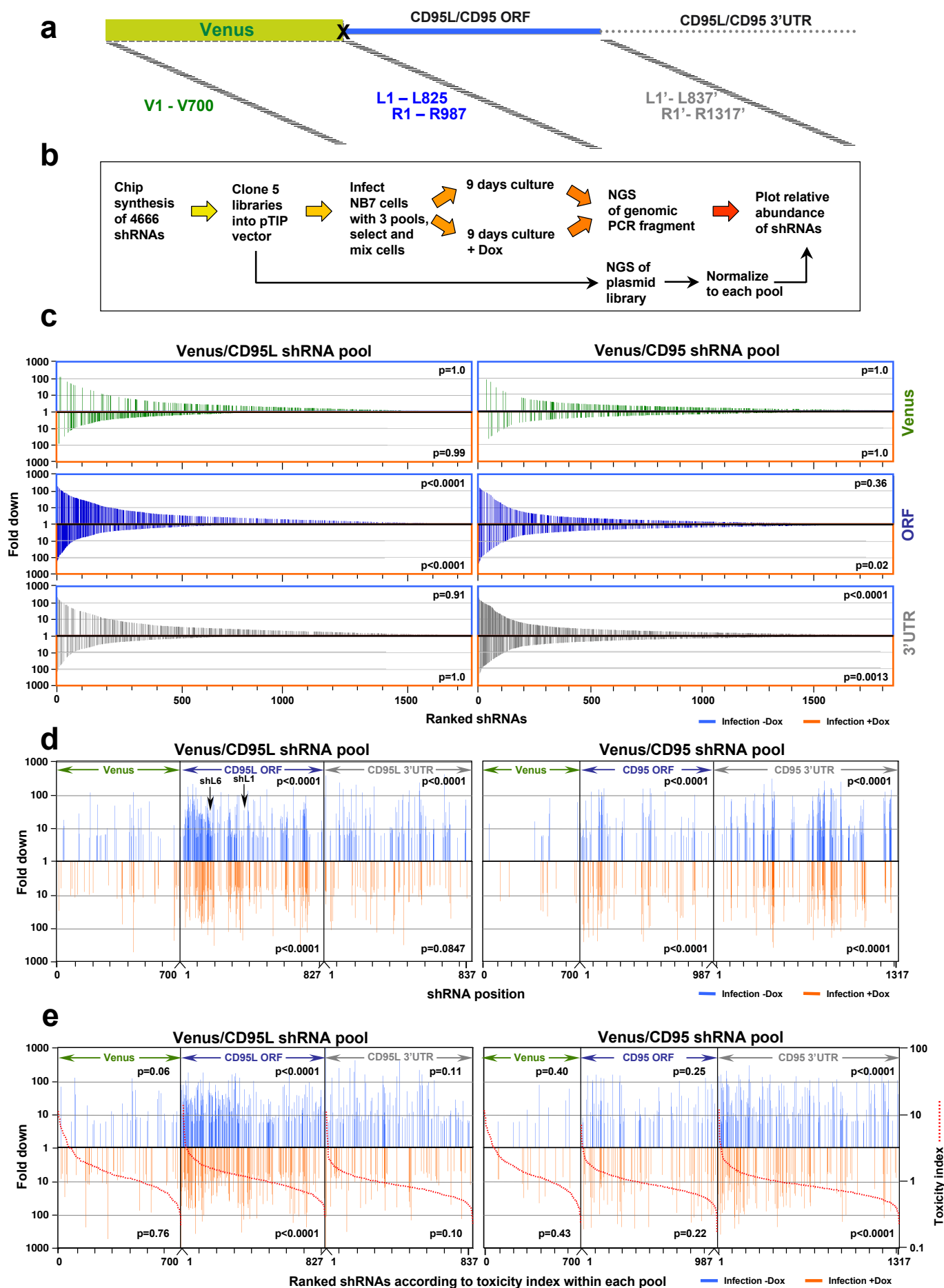


Figure 5

